AN ABSTRACT OF THE THESIS OF

Guido Gold for the degree of Master of Science in Physics presented on October 17, 1985.

Title: Critical Exponents of Sputtered Amorphous $Gd_{0.70}$ $Pd_{0.30}$

Abstract approved: Redacted for Privacy
David J. Griffiths

The magnetization of amorphous $Gd_{0.70}$ $Pd_{0.30}$ prepared via sputtering was measured between temperatures of 100 and 300K and in fields up to 3.5 kOe. The ferromagnetic Curie temperature T_c and the critical exponents β, γ, and δ were found to be 106.29 ± 0.20 K, 0.374 ± 0.04, 1.010 ± 0.05, and 3.915 ± 0.08, respectively. These experimentally determined values,

(1) satisfy the scaling law $\gamma = \beta(\delta-1)$,

(2) are essentially identical to those found for liquid-quenched amorphous Gd-Pd of the same composition, and

(3) provide direct confirmation that critical exponents of a given system are independent of the method of preparation. As in the case of the liquid quenched alloy, γ assumes the value of unity in the neighborhood of the ferromagnetic Curie temperature, T_c, and inverse susceptibility measurements indicate a moment an order of magnitude greater than that associated with single Gd-ions.

Additionally, the set of measured critical exponents predicts a positive value for α, the zero field specific heat exponent. Finally, it is noted that the paramagnetic Curie temperature θ_p is 26 K higher than T_c. It is argued that these results indicate the possible existence of super-paramagnetism in amorphous $Gd_{0.70}Pd_{0.30}$. Wide angle X-ray scattering (WAXS) reveals no measurable crystallinity, but an average Gd-Gd (Gd-Pd) separation distance of 4.47 Å, while the small angle X-ray results (SAXS) indicate the presence of inhomogeneities having an effective radius of 6.5 Å and a mean separation from one another of 50 Å.

Critical Exponents of Sputtered Amorphous $Gd_{0.70}Pd_{0.30}$

by

Guido Gold

A THESIS

submitted to

Oregon State University

in partial fulfillment of
the requirements for the
degree of

Master of Science

Completed October 17, 1985

Commencement June 1986

APPROVED:

Redacted for Privacy

Professor of Physics in charge of major

Redacted for Privacy

Head of department of Physics

Redacted for Privacy

Dean of Graduate School

Date thesis is presented October 17, 1985

Typed by Katherine Haag for Guido Gold

ACKNOWLEDGEMENT

I wish to express my gratitude to Dr. David J. Griffiths who initially proposed the problem described in this thesis, and as a major professor gave support, counsel, and assistance in the completion of this work. It was a great pleasure and privilege to have worked under Dr. Griffiths.

Thanks are also due to Dr. Hollis Wickman (Department of Chemistry) for the use of his susceptibility measuring apparatus, and Ken Sun (graduate student in Chemistry) who gave considerable advice in the beginning stages of the experiment.

I also wish to express appreciation to Dr. John Gardner for his encouragement in doing this thesis.

TABLE OF CONTENTS

LIST OF FIGURES

APPENDIX FIGURES

CRITICAL EXPONENTS OF SPUTTERED AMORPHOUS $Gd_{0.70}Pd_{0.30}$

INTRODUCTION

Many of the basic aspects of critical phenomena were observed fifty or even a hundred years ago, while others have been discovered only in recent years. A primary concern of the more recent 'modern era" of critical phenomena has been the study of critical point exponents in magnetic systems and their description in terms of theoretical models.

Magnetism in structurally amorphous alloys has been the subject of considerable interest, not only as a topic in solid state physics, but also because of its technological potential. Most of the work has been done on 3d transition metal alloys with or without glass formers. The samples are prepared using various techniques such as quenching, different kinds of deposition, and sputtering. These production methods favor a high degree of compositional as well as topological disorder. Amorphous solids are of particular interest in magnetism since they can yield fundamental information on the effect of the formation of magnetic moments and the nature of the exchange interaction.

This thesis describes a standard experiment in which the magnetic susceptibility and magnetic moment of amorphous (sputtered) $Gd_{0.70}Pd_{0.30}$ were determined over a wide temperature range

at small magnetic fields. The choice of Pd and Gd allows the investigation of a rare earth alloy incorporating an element intermediate between early members of the transition group with local moment and a noble metal. In addition, gadolinium being an S-state ion, the alloy chosen is free of any anisotropy field interaction. The initial part of the work describes the determination of the critical point (onset of magnetic ordering) and the critical exponents associated with it. The results of this work are then compared with recent investigations conducted by D. J. Griffiths et al. (ref. 1) on liquid quenched Gd-Pd alloy with the same atomic composition (70 at. % Gd and 30 at. % Pd).

THEORY

Treatment of the theory of phase transitions and critical exponents is far-reaching and to some extent complete. The early papers by Kadanoff et al. (ref. 2), Fisher (ref. 3), and others provided a more recent formulation of the subject, and many review articles now exist which treat all aspects in detail. The general theory of critical exponents is not simple, and a rigorous mathematical treatment is beyond the scope of this thesis. It will be useful, however, to consider some of the basic ideas to provide some insight into this phenomenon.

Qualitative features of critical phenomena

Since much of the following discussion will concern the way in which various physical quantities diverge as the temperature or other variables approach their critical point values, it is appropriate to present a few mathematical definitions which enable critical behavior to be characterized numerically.

One may say a positive function $f(x)$, for example, an equation of state, varies as x^{λ} when x approaches zero from above:

$$f(x) \sim x^{\lambda} \quad \text{as} \quad x \to 0^{+} \tag{1}$$

More precisely this will mean that

$$\lambda = \lim_{x \to 0} \frac{\ln f(x)}{\ln x} \tag{2}$$

The existence of the point exponent λ does not mean that $f(x)$ is simply proportional to x^{λ}. In what might be termed a simple case, one may hope that this will be of the form

$$f(x) = A\, x^{\lambda} \{1 + a\, x + ...\} \tag{3}$$

where A is the amplitude of the singularity and

a is the amplitude of the first correction term.

In particular cases, however, the correction term may be large or may be of a more singular form, so that the leading asymptotic behavior is less easily resolved.

In a non simple case, complexities such as

$$f(x) = A\, x^{\lambda} \mid \ln x \mid^{\mu} \{1 + a\, x + ...\} \tag{4}$$

might arise without contradicting equations (1) and (2). If this occurs it may be very difficult if not impossible to estimate the leading term from numerical data.

Thermodynamic Properties at the Onset of Magnetic Ordering

A ferromagnetic material is characterized by the onset of a spontaneous magnetization as the temperature T drops below the critical point T_c.

$$M_0(T) = \lim_{H \to 0} M(H,T) \tag{5}$$

where H will always denote the 'true' or 'internal' magnetic field acting upon the system (i.e. the applied field, corrected for demagnetization). Above T_c in the paramagnetic region the magnetization varies continuously as H changes sign.

The observed magnetization at zero field just below T_c is well described by the power law:

$$M_0(T) \sim |T - T_c|^{\beta} \quad \text{for } T < T_c \tag{6}$$

where β is sometimes called the magnetic exponent.

The onset of ordering is signaled as the temperature drops to T_c from above, most notably by the zero field susceptibility. In the absence of magnetic interactions the magnetic susceptibility varies with T according to:

$$\chi = C/T, \text{ with } C = \frac{N\mu_B^2}{3Vk_B}\mu_{eff}^2 \qquad \underline{\text{Curie Law}} \tag{7}$$

with the effective magnetic moment

$$\mu_{eff} = g(JLS)[J(J+1)]^{1/2} \tag{8}$$

In a ferromagnet, however, the initial isothermal susceptibility

$$\chi_0(T) = \left.\frac{\partial M(H,T)}{\partial H}\right|_{T = \text{const.}} \tag{9}$$

diverges as T_c is approached following the power law:

$$\chi_0(T) \sim (T - T_c)^{-\gamma} \quad \text{for } T \to T_c^+ \tag{10}$$

This is a generalization of the Curie-Weiss Law, which, based on the mean-field approximation (ref. 4) predicts a value of $\gamma = 1$

(ref. 5). Symmetry with respect to H below T_c means that one need only define a single exponent γ for the divergence of the $\chi_0(T)$

$$\chi_0(T) \sim (T_c - T)^{-\gamma'} \quad \text{for } T \to T_c^- \tag{11}$$

Equation (10) and (11) imply that $\gamma = \gamma'$.

A similar characteristic divergence is observed in the zero field specific heat above and below the critical point:

$$C_0(T) \sim (T - T_c)^{-\alpha} \quad (T \to T_c^+) \tag{12}$$

$$C_0(T) \sim (T_c - T)^{-\alpha} \quad (T \to T_c^-) \tag{13}$$

This singularity is not nearly so strong as the initial susceptibility.

The behavior at the critical point is characterized through the critical isotherm. The singularity in M is sufficiently described by considering only the leading term in the magnetic equation of state:

$$H \sim \text{sgn}\{M\}\ M^{\delta} \quad \text{at} \quad T = T_c \tag{14}$$

At this point one might rightfully question, why one should focus on a quantity such as the critical point exponent, which contains considerably less information than the complete functional form. The answer seems to lie in the experimental fact that near the critical point the behavior of the leading term dominates.

Basis of the Scaling Law Hypothesis

Much experimental and theoretical work on critical phenomena seems to support the idea that there exist simple relationships among different exponents. When these relationships are derived on the basis of the mechanical stability criterion (in thermodynamics) they turn out as inequalities. In many cases, however, they are satisfied as equalities rather than inequalities. Although no one has rigorously proven this, an alternate approach, known as the 'static scaling law' or 'homogeneous function approach', has been rather successful.

The static scaling hypothesis asserts that thermodynamic potentials are homogeneous functions. In the case of the Gibbs' free energy, specified for magnetic systems, that is:

$$G\ (\lambda^{a_\varepsilon}\varepsilon,\ \lambda^{a_H}H) = \lambda G\ (\varepsilon,H) \tag{15}$$

the temperature has been replaced by the reduced temperature $\varepsilon = (T - T_c)/T_c$; a_ε, a_H are arbitrary parameters, and λ can be any number.

Differentiating both sides of equation (15) with respect to H gives:

$$\lambda \partial G\ (\varepsilon,H)/\partial H = \lambda^{a_H}\ \partial G\ (\lambda^{a_\varepsilon}\varepsilon, \lambda^{a_H}H)/\partial(\lambda^{a_H}H) \tag{16}$$

Since the partial derivative is the negative of the magnetization, equation (16) is, after rearranging, equivalent to

$$M(\varepsilon,H) = \lambda^{a_H - 1} M\,(\lambda^{a_\varepsilon}\varepsilon, \lambda^{a_H} H) \tag{17}$$

At the critical point, however, the exponents β and δ are related to $M\,(\varepsilon,0)$ at $H = 0$ as $\varepsilon \to 0$, and $M\,(0,H)$ at $\varepsilon = 0$ as $H \to 0$. respectively. This allows one to specify the exponents in terms of the unknown scaling parameters a_ε, and a_H

$$\beta = (1 - a_H)/a_\varepsilon \tag{18}$$

$$\delta = a_H/(1 - a_\varepsilon) \tag{19}$$

with the particular choice of $\lambda = (-1/\varepsilon)^{1/a_\varepsilon}$ and $(H)^{-1/a_H}$ respectively. Additional exponents are obtained by taking higher order derivatives of (15) that are related to other variables which diverge at the critical point. In such a way, the critical exponent γ can be found similarly to β as:

$$\gamma = (2a_H - 1)/a_\varepsilon \tag{20}$$

Solving equations (18) and (19) simultaneously and combining with (20) results in:

$$\gamma = \beta\cdot(\delta - 1) \tag{21}$$

known as the Widom equality, which initially has been established by thermodynamic considerations as an inequality (for a more detailed analysis see Stanley, ref. 6, Chapters 4 and 11). Various relationships can thus be found, such as the Griffiths inequality which is satisfied as an equality and combines a different set of exponents.

$$2 = \alpha + \beta\cdot(\delta + 1) \tag{22}$$

The fact that all the critical point exponents can be expressed in terms of only 'two' scaling parameters a_ε and a_H means that if two exponents are specified, virtually all others can be determined.

Determination of the Critical Exponents

The critical exponents will be determined using equations (6), (10), and (14) from above. A conventional technique developed by Arrott (ref. 7) and Kouvel (ref. 8) was to plot the data at various temperatures as M^2 vs. H/M. In practice, above the critical point, χ_0^{-1} (inverse initial magnetic susceptibility) is found as the intercept on the H/M axis in the limit of zero magnetic field when extrapolated to $M^2 = 0$. At $T > T_c$, $\chi_0^{-1} = H/M$ as $M^2 \to 0$ which is equivalent to H = 0. Below the critical point, in the ferromagnetic regime, the intercepts along the M^2 axis, that is H/M = 0 (for the respective isotherms), give the squares of the spontaneous magnetization M_0^2. Differentiating equation (10) with respect to T gives

$$\frac{d\chi_0^{-1}}{dT} \sim \gamma (T - T_c)^{\gamma-1} \tag{23}$$

and may be further rewritten as:

$$\frac{\chi_0^{-1}}{d\chi_0^{-1}/dT} \sim \gamma^{-1} (T - T_c) \tag{24}$$

A similar expression results from equation (6) for the spontaneous magnetization:

$$\frac{M_0}{dM_0/dT} \sim \beta^{-1} (T_c - T) \tag{25}$$

In plots of χ_0^{-1} vs. T and M_0 vs. T, the gradients $d\chi_0^{-1}/dT$ and dM_0/dT respectively have to be approximated as finite differences around each data point. These values are further used for plots of $\chi_0^{-1}/\{d\chi_0^{-1}/dT\}$ (T) and $M_0/\{dM_0/dT\}$ (T). The inverse of the slopes (at least in a finite range of ordinate) are the exponents γ and β respectively. The intercept with the T axis determines in each case the critical temperature T_c. Finally, the exponent δ, which was defined for the critical isotherm, is determined by a plot of log(M) vs. log(H) at $T = T_c$.

APPARATUS

These investigations were conducted by means of a Faraday balance utilizing a six-inch electromagnet with a set of Lewis gradient coils mounted on its pole faces. The major components were fixed on a concrete base in order to isolate the system from noise mainly due to the lab environment. This experimental setup is capable of measuring both magnetic susceptibility and magnetic moment of a given sample when placed in the center of an applied d.c. magnetic field and gradient field. A picture of the apparatus is shown in FIGURE 1.

The Cahn Electrobalance

The balance used to measure the apparent weight gain and weight loss of the sample respectively is based on the null - balance principle. When the sample weight changes the beam tends to deflect momentarily. The flag, suspended on one side of the beam, moves with it changing the intensity of light to the phototube and consequently its phototube current. This current is amplified in a two-stage servo amplifier and applied to a coil which is in a magnetic field (FIGURE 2). The coil acts like a d.c. motor exerting a force on the beam to restore it to the original balance position. Thus the change in electromagnetic force is equal to the change in sample weight. In this way the beam is always kept in dynamic equilibrium since the electromagnetic restoring force is exactly proportional to the current which causes it.

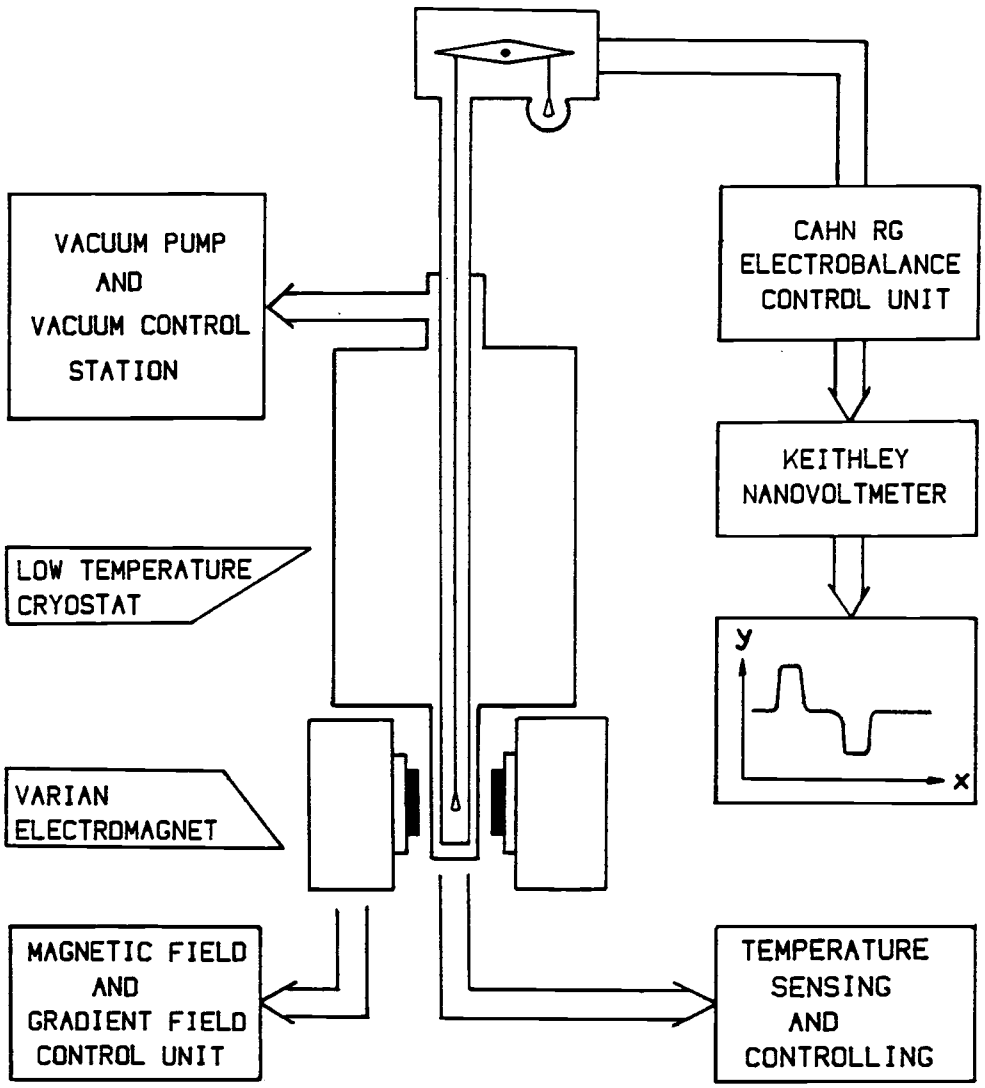

FIGURE 1: Diagram of the magnetic susceptibility apparatus

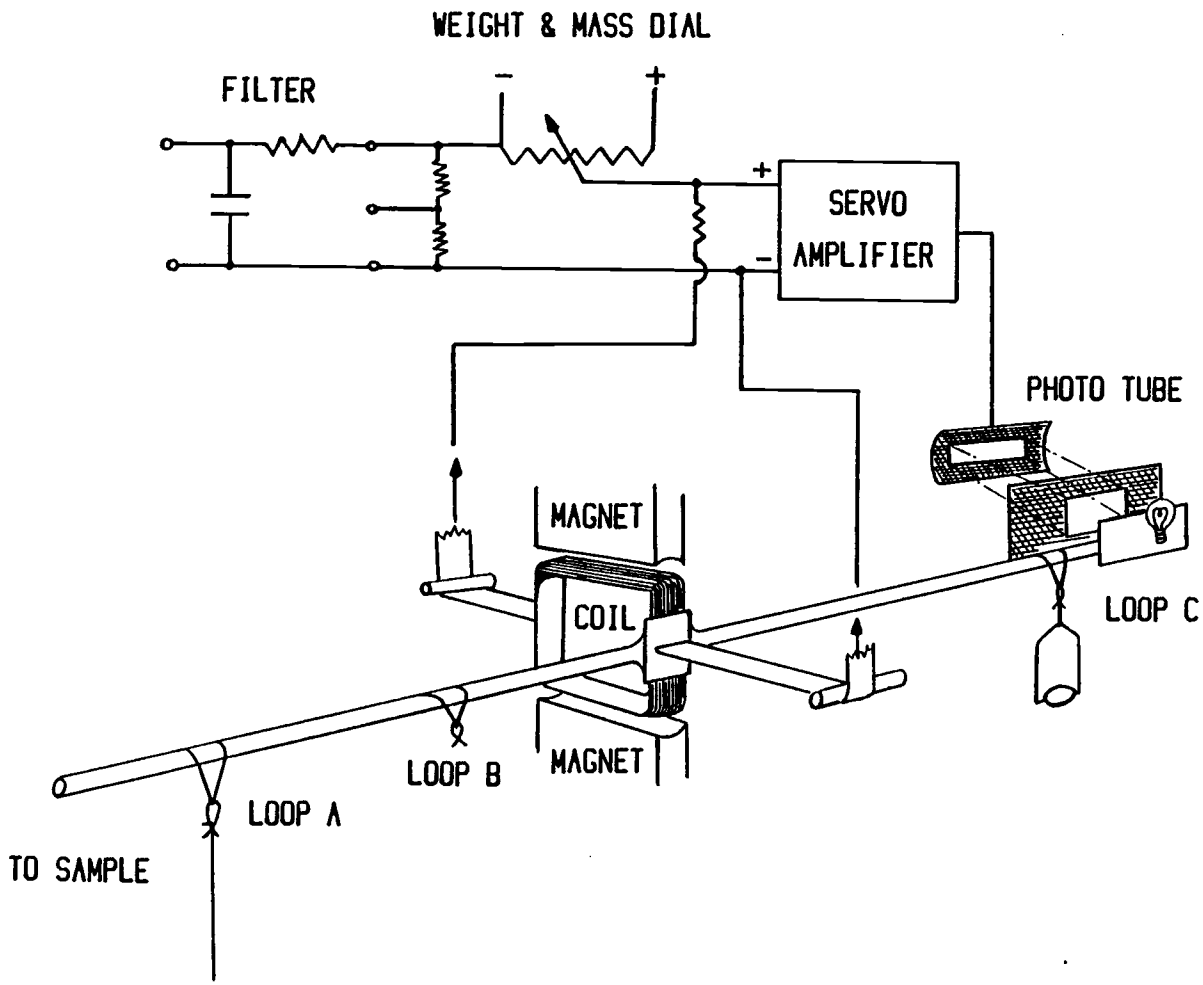

FIGURE 2: The Cahn automatic electrobalance

In order to use a practical recorder or simply to display. it is necessary to subtract and measure a part of the voltage with circuits inside the balance, and only apply the excess to the recorder device. Thus a known, accurately calibrated voltage is subtracted from the voltage across the coil, by means of an accurate potentiometer. A dial on the potentiometer reads directly in milligrams, corresponding to the amount of voltage subtracted in the circuit. The excess of coil voltage over reference voltage is then available for the recorder, or intermediately for a precise voltmeter. In our case a Keithley nanovoltmeter is being used. By attenuating the voltage input by known ratios, various weight ranges can be displayed and easily translated into grams or small fractions thereof, taking the apparatus settings of balance plus nanovoltmeter into account. The maximum resolution of the apparent weight change, given by the balance settings is 0.02 μg, which in practice is reduced to about 1 μg, essentially due to external noise and static electricity on the sample hangdown.

The output of the nanovoltmeter is, in addition, connected to an X - Y recorder which provides another way of recording the apparent weight change of the sample. The latter feature turned out particularly useful when working with high sensitivities.

Low Temperature Cryostat

A standard three-chamber cryostat (FIGURE 3) has been used for low temperature measurements, allowing the use of liquid Helium and

Nitrogen as low temperature media. A central chamber 'A well' hosts the sample tube with dimensions of approximately 40-1/2" in length and 1/2" in diameter. Thermal contact between the otherwise separated chambers is made possible through a needle valve, installed at the bottom of the B well. This valve is manually operated at the top outside the cryostat; thus the flow of Nitrogen or Helium gas can be controlled and a coarse temperature set.

The Electromagnet and Gradient Coils

The field exerted on the sample is supplied by a six-inch Varian electromagnet. A uniform d.c. magnetic field, up to 5.75 kOe, can thus be established.

In order to deflect the sample vertically, a pair of Lewis gradient coils is mounted on the magnet pole faces. This allows a rapid reversal of the gradient for a given field value in a matter of seconds (thereby eliminating any spurious d.c. bias in the signal). The gradient field is controlled by a variable solid state power supply with a maximum current output of about 30 Amp which corresponds to a gradient value of 207.12 Oe/cm.

Both d.c. magnetic field and gradient field are detected by a Hall probe whose voltage output is displayed on a HP - digital multimeter.

Temperature Sensing and Controlling

For temperature measurements a Lake Shore Cryotronic temperature controller was available with a control accuracy of 0.005 K

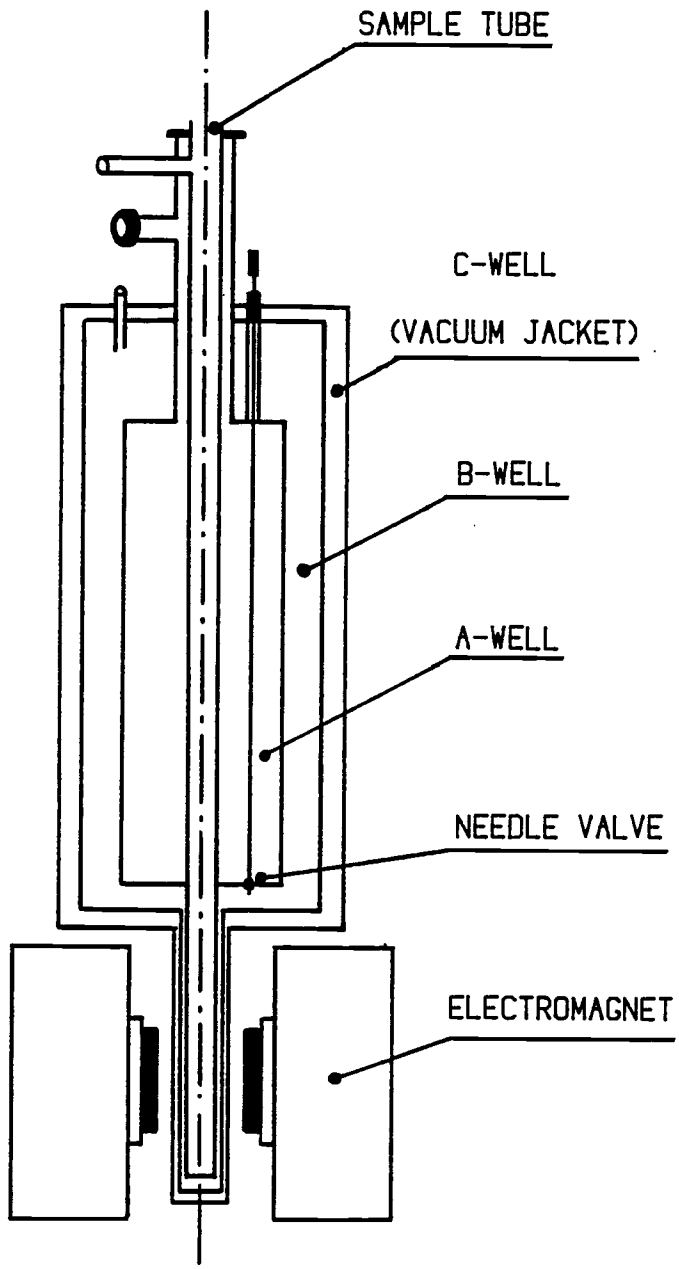

FIGURE 3: Low temperature cryostat

between temperatures of 28 and 400 K. The thermometers, a Si- and GaAs-diode (Lake Shore Cryotronics, DT-500 series) have been installed at the bottom of the sample tube, in the neighborhood of the sample. A schematic of the temperature control/sensing unit is shown in FIGURE 4.

The GaAs-diode serves as a control diode and is biased by a 10 microamp d.c. precision current source built into the control unit. A voltage can be set externally on the control panel. This digital set point which corresponds to a specific temperature is converted to an analog voltage by a D/A converter. The resulting voltage is negative and an appropriate resistance string is chosen so that its current into a summing amplifier just balances the sensor generated positive current. The result is zero current at the summing junction when the set point voltage is just equal to the sensor voltage. When this current is unequal to zero the difference is then interpreted as an error signal. Its integral and differential are summed as current by an operational amplifier. This amplifier drives the output power circuit to which a heater element has been connected.

Here is some of the logic: When the set point is lower than the voltage sensed by the diode, the heater is turned off and the temperature has to be adjusted externally by regulating the flow of cold N_2 gas in the cryostat. Assuming the set point is too high, the heater is turned on and the temperature will be raised.

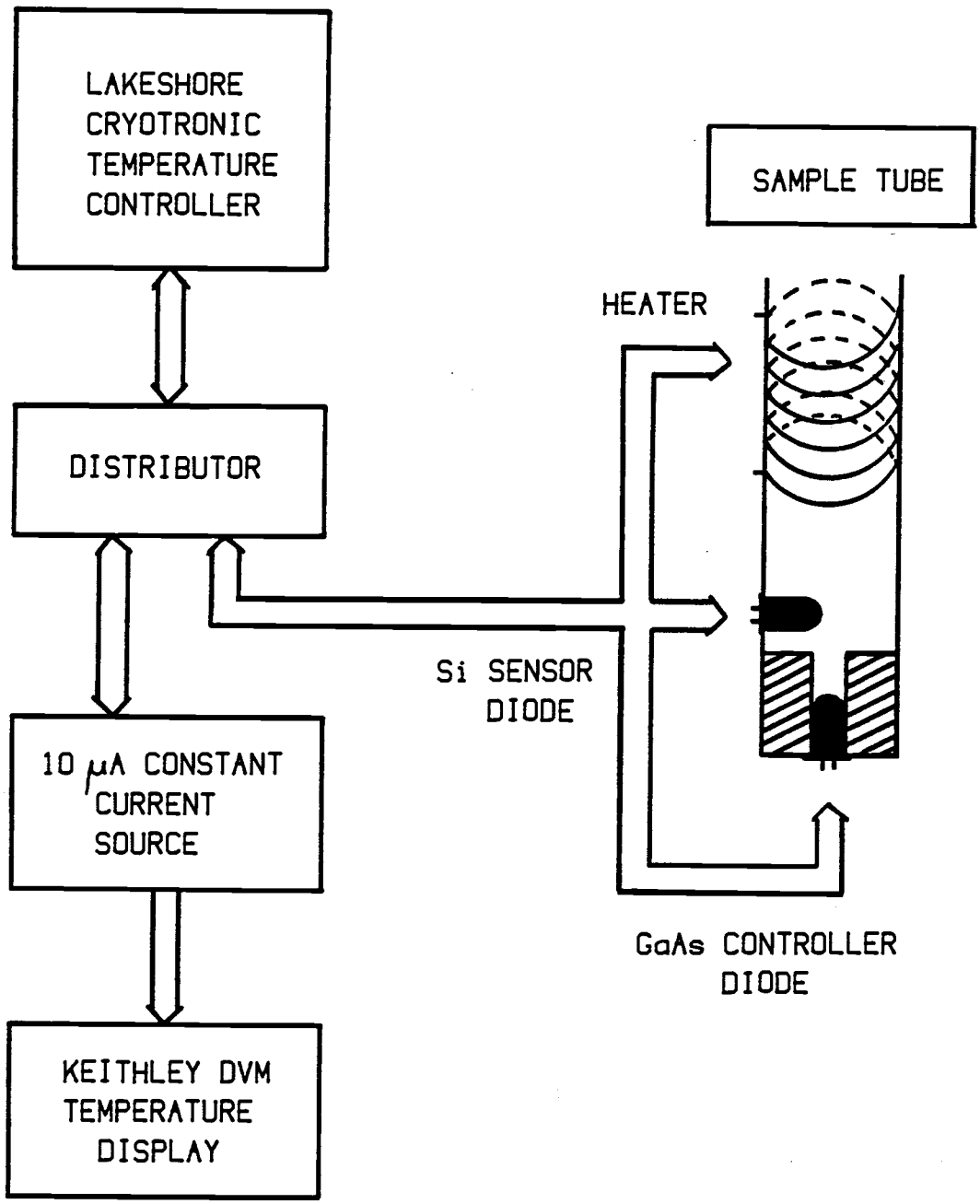

FIGURE 4: Block diagram of the temperature control unit

The Si-diode which is supplied by an independent current source is used as the final temperature sensing device and its voltage is displayed on a five digit Keithley multimeter. With appropriate calibration, the recorded signal can easily be translated into a temperature.

EXPERIMENTAL PROCEDURE

Before suspending the hang-down with sample in the sample tube a weak ionization source (α particles from ^{210}Po) was used to irradiate the quartz bucket and sample. A small piece of the Polonium isotope was permanently left inside the sample chamber. This should serve to reduce static electricity and related friction effects, which could result in excessive noise on the recorder, especially on dry days. The electrobalance and attached hangdown were then adjusted so that the quartz bucket with sample could hang freely without touching the walls of the surrounding tube.

After evacuating balance and sample chamber these were flushed with dry Helium (g) after which a pressure of 5-10 mm Hg of Helium was left to serve as a heat exchange gas. Subsequently the cryostat was evacuated and the main chamber (B-well) filled with liquid Nitrogen (see FIGURE 3).

At this point the apparatus was set for operation.

OPERATIONAL TESTS

Operational testing of the apparatus consisted of a thorough calibration of the balance and the temperature sensing Si - diode prior to its use. In addition the gradient field value was verified. In this section only the balance calibration will be treated. The temperature - and gradient field calibration will be discussed in Appendix 3.

Mercury tetrathio-cyanato-cobaltate (II), $[HgCo(SCN)]_4$, with known magnetic susceptibility, is a common calibrant for magnetic susceptibility measurements especially because of its simple and well known temperature dependence. Since the compound exists in powdered form it had to be packed in NBS aluminum foil in order to avoid its spreading into the sample tube.

The measurements were conducted over a range of temperature of about 80 - 240 K at a constant magnetic field of 3.95 kOe. In the data evaluation the paramagnetic susceptibility of the Al packing foil and the diamagnetic contribution due to the quartz bucket had to be taken into account according to:

$$\chi_m = \frac{g\ (\Delta m - \Delta m_{QB})}{2 m_s H\ \{dH_x/dz\}} - \chi_m^{Al}(T) \qquad (26)$$

χ_m is the mass specific susceptibility, not the χ customarily found in classical electromagnetic theory. Δm and Δm_{QB} denote the apparent change of mass of the sample and quartz bucket respectively; m_s is the sample mass itself, H is the applied magnetic field, and dH_x/dz is the gradient field responsible for

the vertical deflection of sample and hangdown (for a detailed discussion of equation (26) see Appendix 1). The result of the calibration is shown in Figure 5. The experimental results measured at different days were compared with the known result (ref. 9) and (ref. 10) of

$$\chi_m = \frac{4.985*10^{-3}}{(T + 10)} \ [cm^3\ g^{-1}] \qquad (27)$$

In this way an uncertainty in χ_m of not greater than $\pm\ 1.3*10^{-6} cm^3/g$ was ascertained. Errors in temperature, associated with insufficient energy transfer from the coolant to the sample, and difficulties to stabilize a fixed temperature setting, were estimated as ± 0.15 K.

A further test of the balance was carried out, however, this time at zero magnetic field and at room temperature only. Equal weights were suspended on either side of the balance beam, and a baseline was drawn on the X - Y recorder for different balance settings. Simultaneously the nanovoltmeter response was recorded. This test was repeated by adding a precise 1 mg NBS weight on the stirrup of Loop A (see also FIGURE 2). Both, X - Y recorder chart and electrobalance reading were evaluated and compared with the actual test weight. In either case an uncertainty smaller than 1.5% was established. This simple method might be particularly powerful for quick checks of the balance and recorder response in the course of large scale experiments.

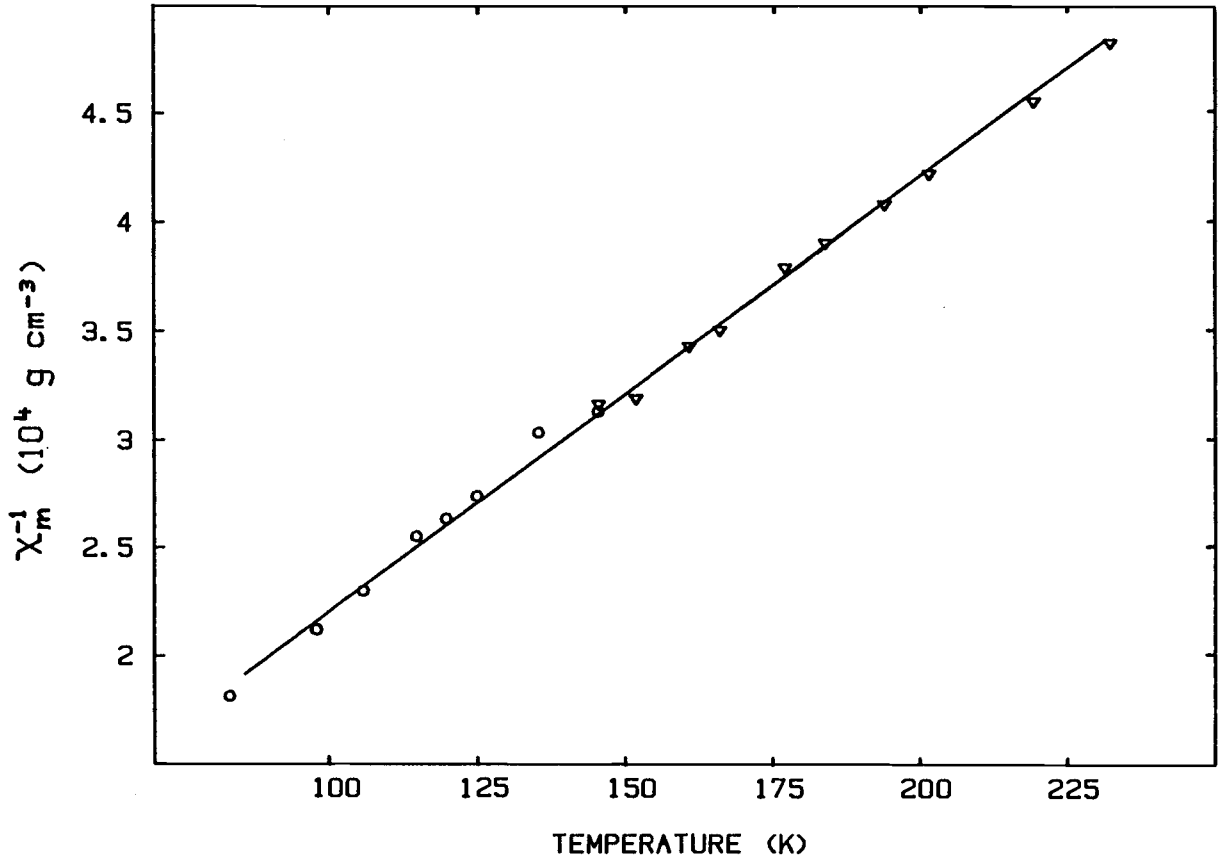

FIGURE 5: Calibration curve for $[HgCo(SCN)]_4$

EXPERIMENTAL MEASUREMENTS

Sample and its Preparation

Samples in the form of small foils having a thickness of approximately 40 μm were produced by B. Boucher and R. Tourbot, at CEN (Centre d'Etude Nucleaire) - Saclay, France, by rapid d.c. sputtering. The structure of the sample was checked by conducting small and wide angle X-ray scattering measurements with Cu Kα radiation. The results, shown in FIGURES 6, 7, and 8, reveal that no measurable crystallites were present and the sample was "truly amorphous" (see discussion section).

For the susceptibility and magnetization measurements specimens were circularly shaped (diameter of about 5 mm) and oriented such that their demagnetization factor was essentially zero.

At temperatures between 295 K and 101 K, the magnetic susceptibility and magnetization were determined. For all temperatures well above the Curie point the sample gave a linear magnetization response at the measured values of applied field ($H < 3.5$ kOe). The results of the M(H) plots, shown in FIGURE 9, are indicative that no saturated component contributes to the total magnetization of the sample. In other words, no crystalline inclusions seemed to be present, a phenomenon commonly observed and discussed in previous investigations on liquid quenched amorphous materials (ref. 1) and (ref. 11).

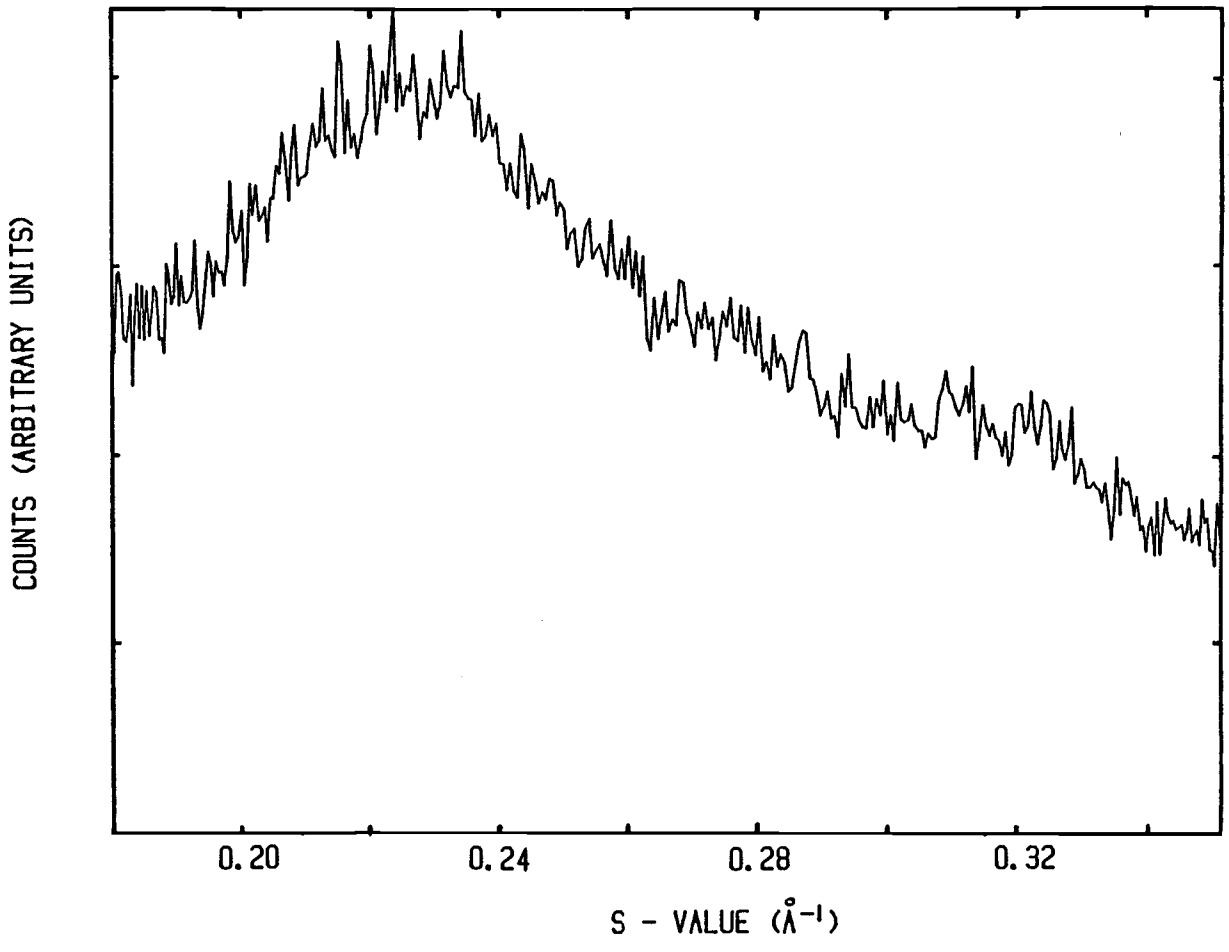

FIGURE 6: Wide angle X-ray scattering on sputtered amorphous $Gd_{0.70}Pd_{0.30}$

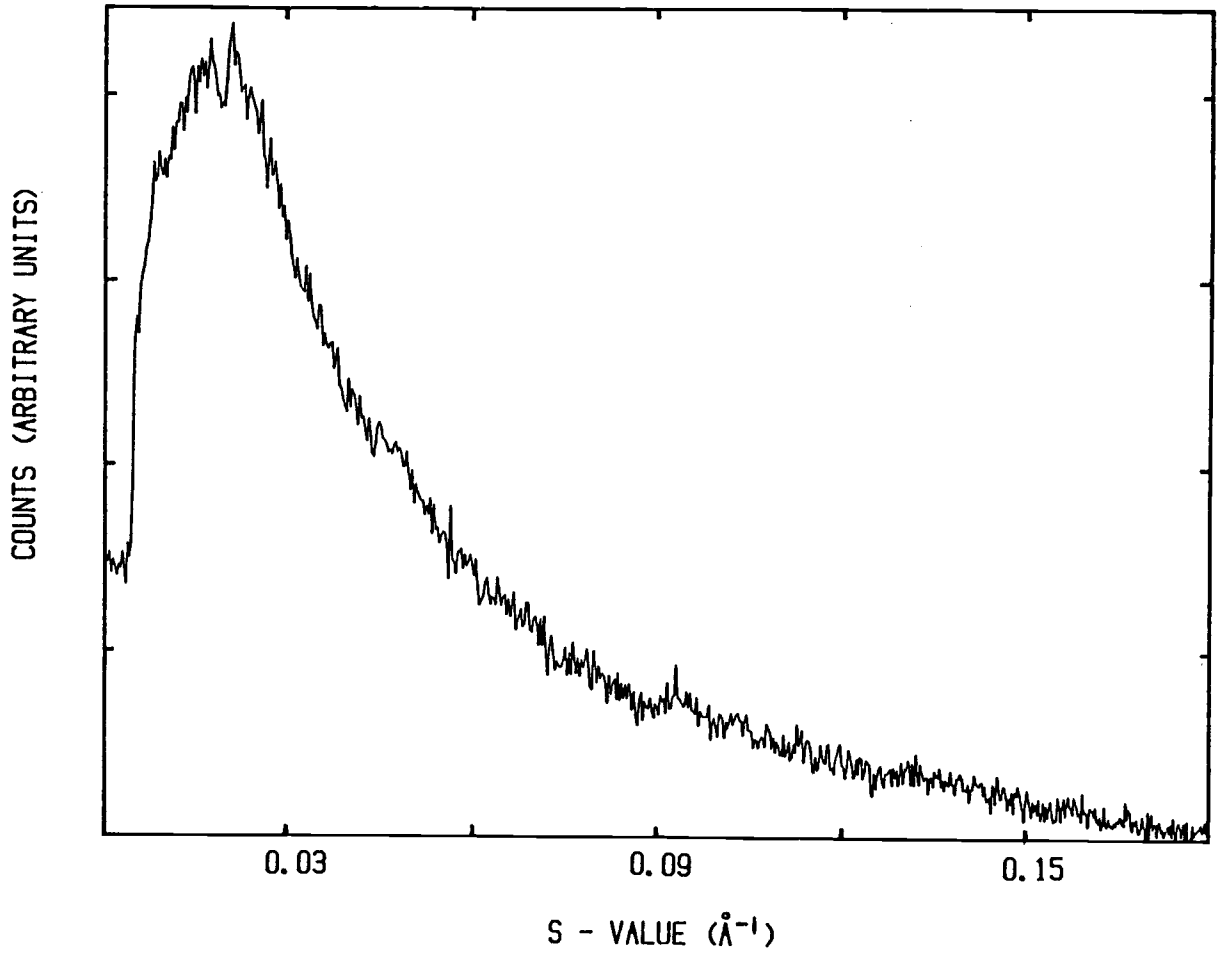

FIGURE 7: Small angle X-ray scattering on sputtered amorphous $Gd_{0.70}Pd_{0.30}$

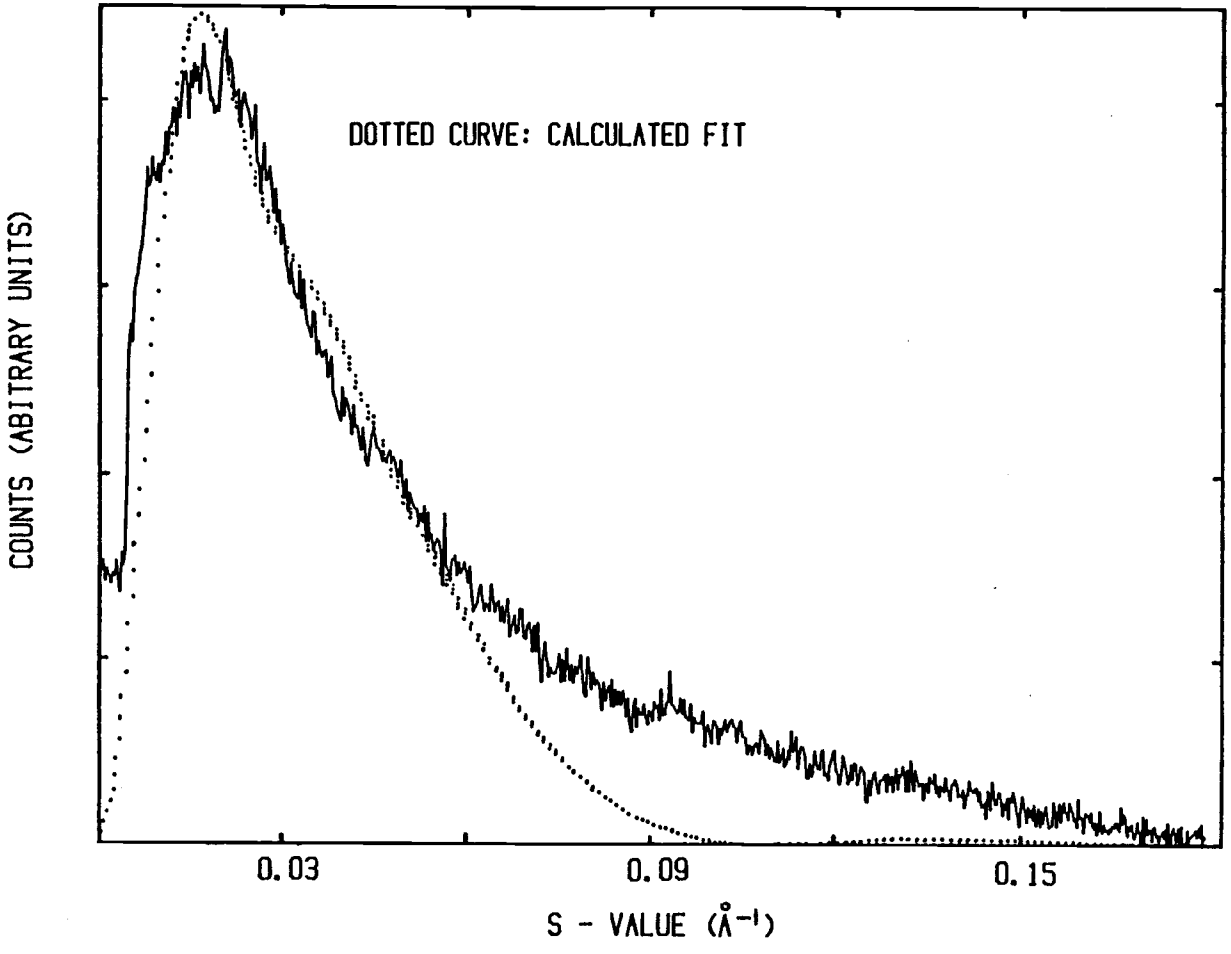

FIGURE 8: Calculated fit for the small angle X-ray trace, in comparison with the experimental trace

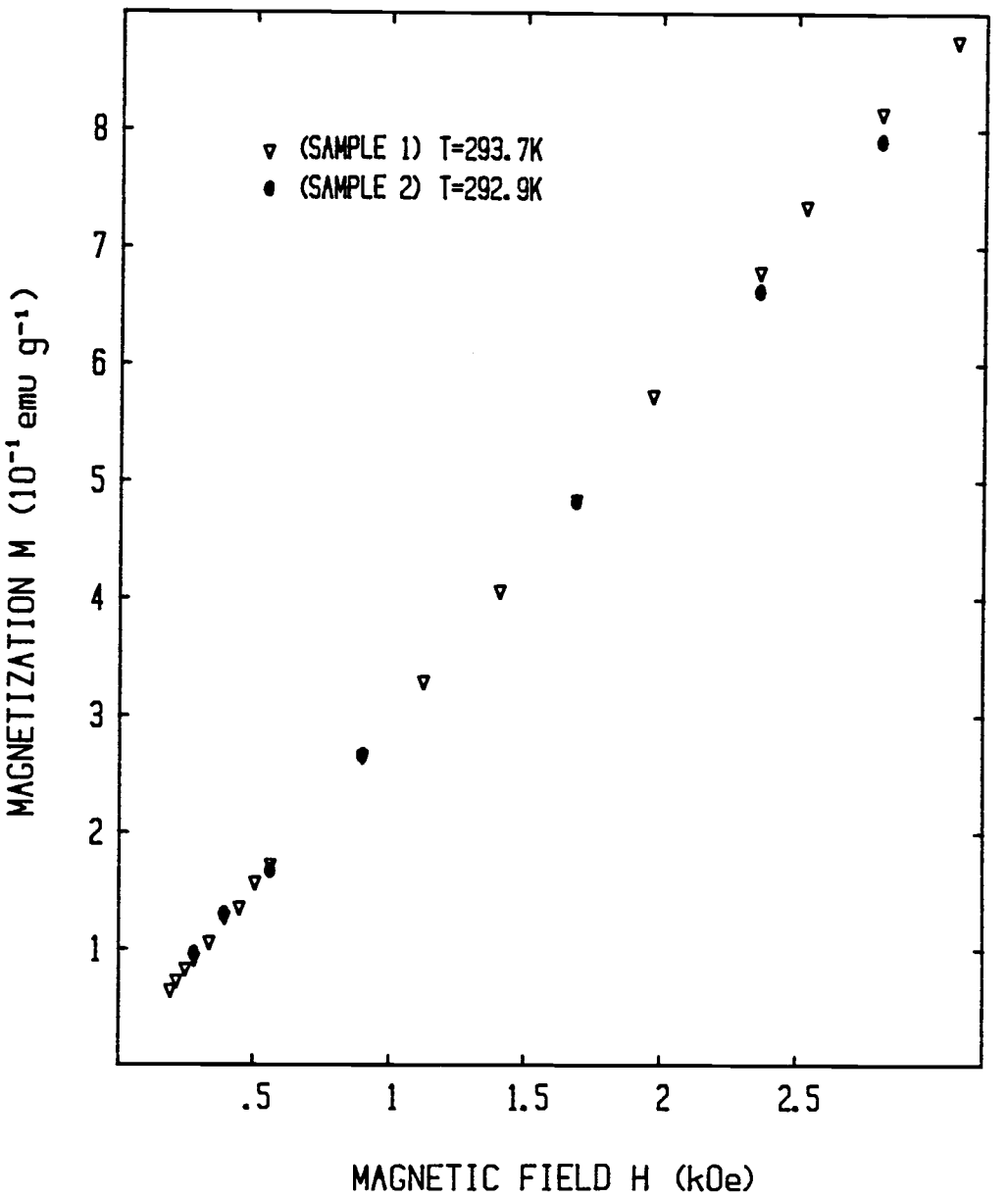

FIGURE 9: M(H) curve for different portions of the sputtered amorphous $Gd_{0.70}Pd_{0.30}$ sample

Results of the Measurement

Over a wide temperature range (200 K) the inverse mass specific susceptibility was plotted against absolute temperature. FIGURE 10 shows that χ_m^{-1} is linear for $T \gg 195$ K. A least mean square fit for this region gives $\chi_m^{-1} = 21.4640 * T - 2837.6766$, resulting in a paramagnetic Curie point $\theta_p = 132.20$ K, and a slope $d\chi_m^{-1}/dT$ of 21.464 $g \cdot cm^{-1} K^{-1}$.

Assuming that Pd does not contribute to a local moment. the significant contribution to the overall magnetic moment has to be due to Gd ions only. In an earlier work on amorphous La-Pd (ref. 12) this has been clearly indicated. Under this assumption one can show that

$$g^2 = \frac{3\ k_B}{N_A \mu_B^2 J(J+1)\{d\chi_m^{-1}/dT\}} [M_{Gd} + (1/x - 1)\ M_{Pd}] \qquad (28)$$

with an effective magnetic moment of

$$\mu_{eff} = g\ [J(J+1)]^{1/2} \qquad (29)$$

where M_{Gd} and M_{Pd} are the respective gram atomic weights, x is the atomic fraction of gadolinium with J = 7/2. Inserting the numbers gives g = 2.190 and μ_{eff} = 8.69 Bohr magnetons. The difference of $\Delta \sim 0.75\ \mu_B$ compared to the free Gd-ion ($\mu_{eff} = 7.94\ \mu_B$) seems to arise from conduction electrons of both gadolinium and palladium ions.

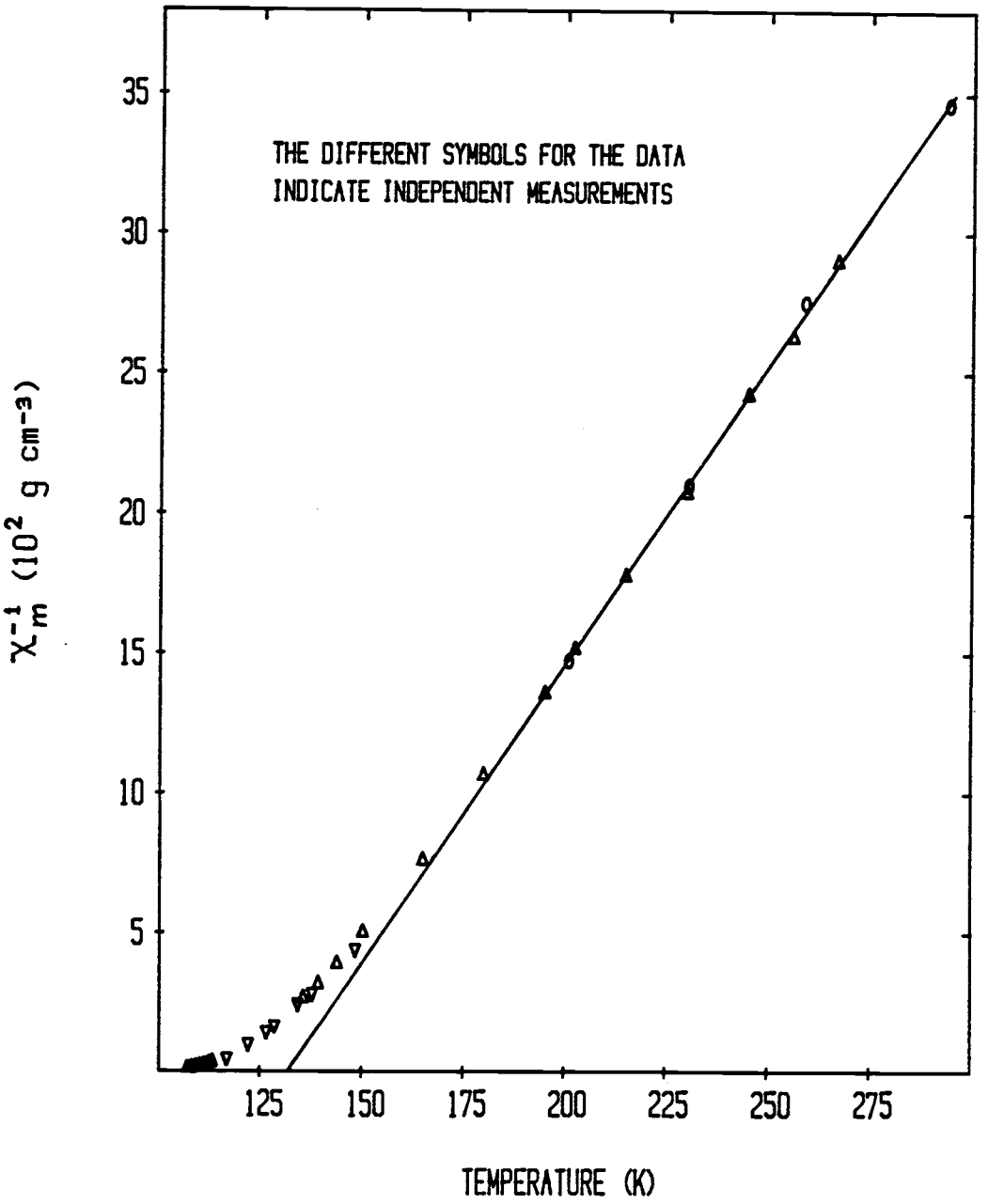

FIGURE 10: Curie Weiss plot of χ_m^{-1} vs. T for sputtered amorphous $Gd_{0.70}Pd_{0.30}$

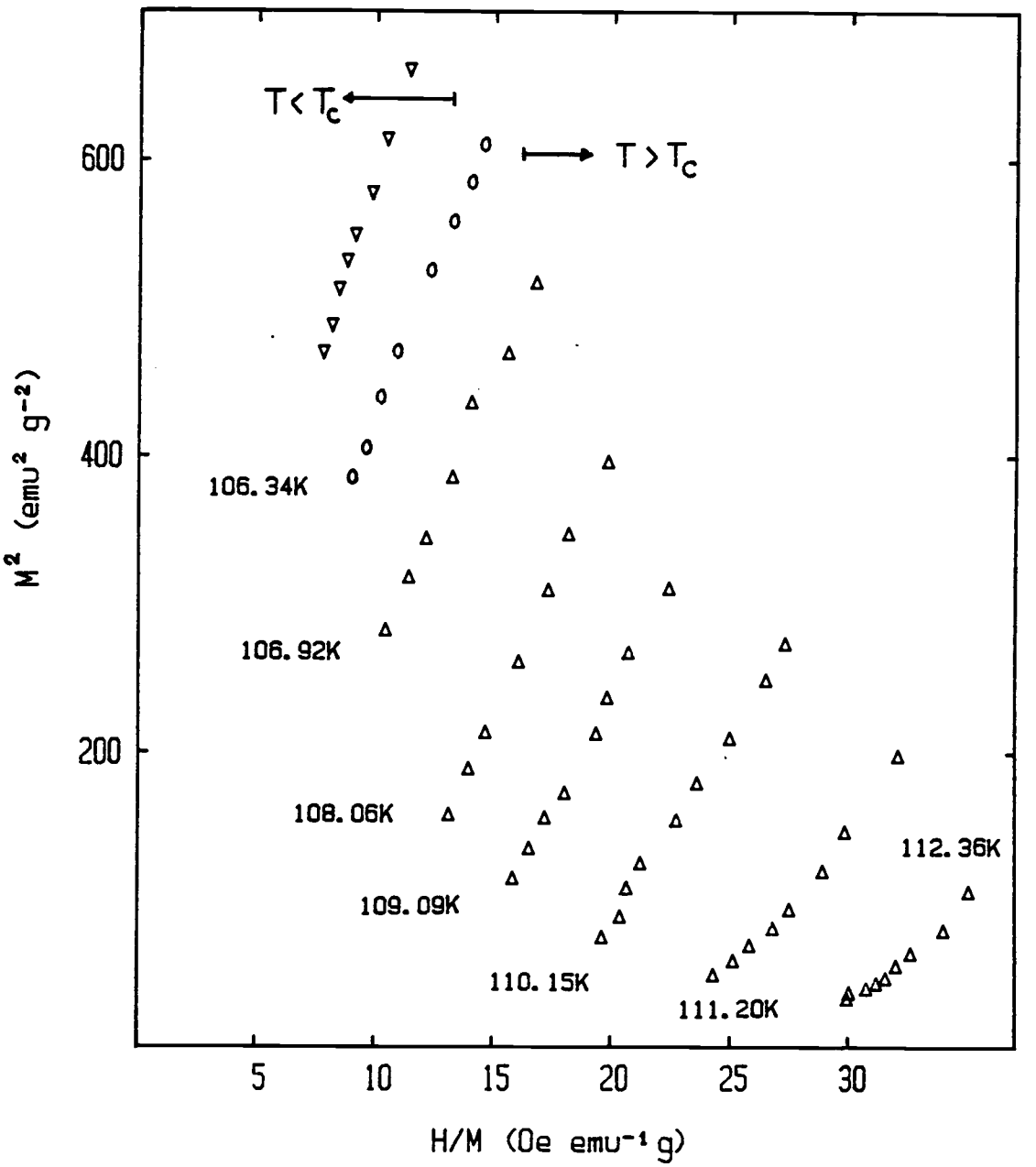

FIGURE 11: Arrott-Kouvel plots for temperatures $T \geq T_c$

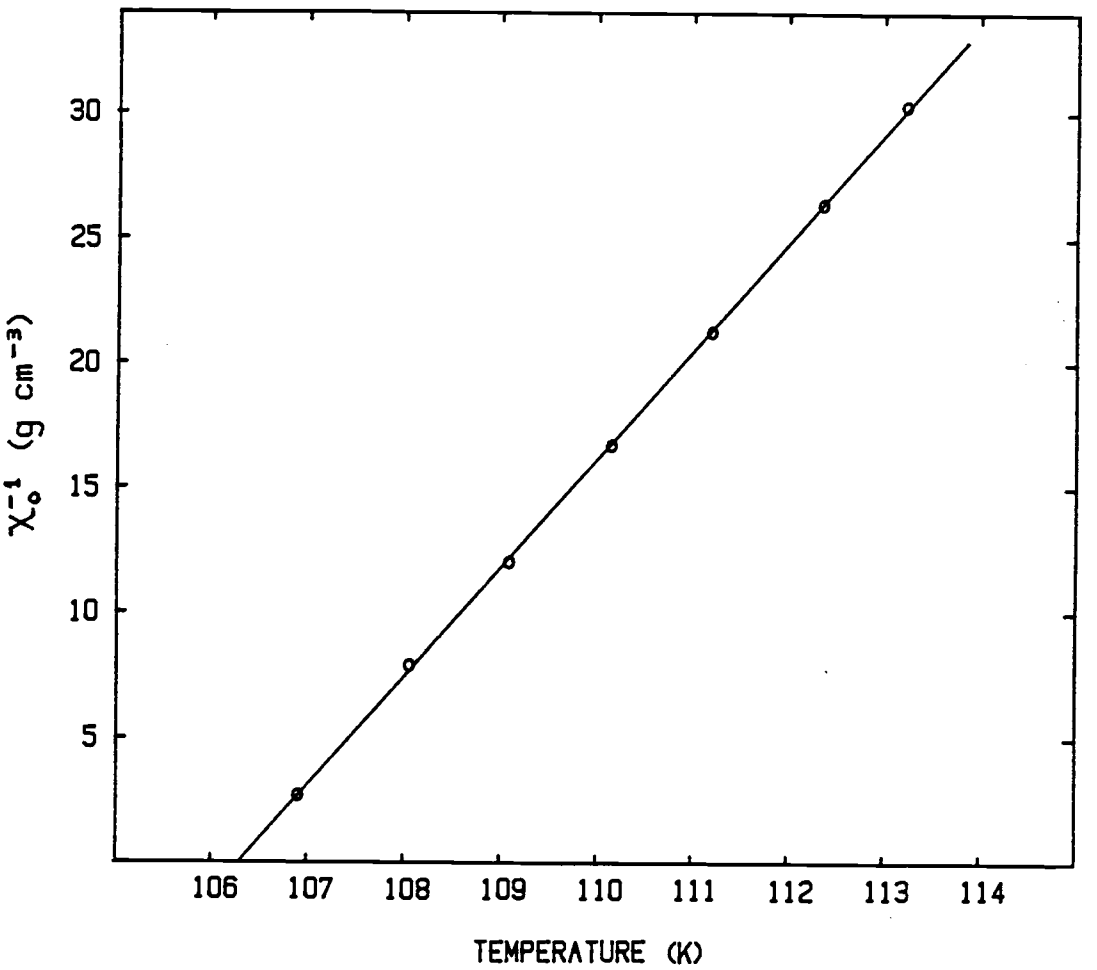

FIGURE 12: Inverse initial susceptibility vs. temperature in the neighborhood of the critical point

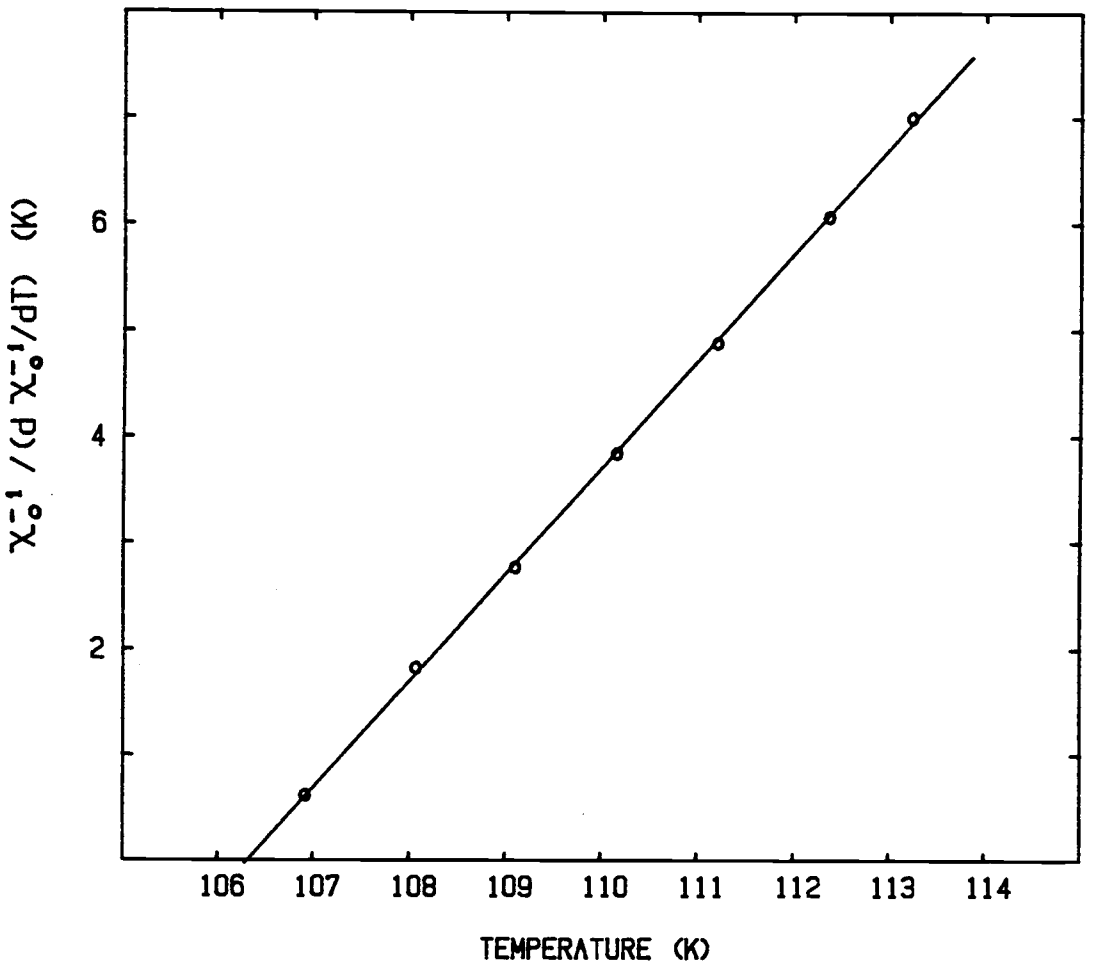

FIGURE 13: $d\chi_0^{-1}/\{d\chi_0^{-1}/dT\}$ vs. T for the amorphous $Gd_{0.70}Pd_{0.30}$ sample in the vicinity of T_c. Least-mean-squares fit to the data gives: $d\chi_0^{-1}/\{d\chi_0^{-1}/dT\}=0.9895*T-105.1858$ with $r^2=0.9998$ resulting in $\gamma=1.010$ and $T_c=106.29$ K.

The onset of magnetic ordering near T_c reveals initial susceptibilities about two orders of magnitude higher than the paramagnetic susceptibility at $T \gg \theta_p$. This region was further illuminated by taking measurements in small steps of approximately 1 - 3 K at $T < 130$ K. It is obviously important to guarantee that the previous magnetic history of the specimen will not unduly influence results, and thus, when conducting magnetization measurements in the vicinity of the transition point (both above and below T_c) care was taken to warm the sample well into the paramagnetic regime before returning, at $H = 0$, to a new temperature near T_c.

For temperatures in the vicinity of the transition point M^2 vs. H/M was plotted in order to determine the inverse initial susceptibilities χ_0^{-1}. FIGURE 11 shows Arrott-Kouvel plots for a temperature range $106 < T < 113$ K on a small scale. However, for a more precise extrapolation to $M^2 = 0$, the H/M - as well as M^2 - scale was enormously expanded in order to reduce the margin of error related to this graphical method.

The inverse initial susceptibilities are then plotted against absolute temperature, which is displayed in FIGURE 12. A strong linear dependence of χ_0^{-1} is observed over ~ 8 K predicting a critical exponent γ of close to unity which was confirmed in plotting $\chi_0^{-1}/\{d\chi_0^{-1}/dT\}$ vs. T (FIGURE 13). The functional relationship found by means of a least mean square fit is:
$\chi_0^{-1}/\{d\ \chi_0^{-1}/dT\} = 0.9895 * T - 105.1858$ assigning a $\gamma = 1.010$ and the critical temperature T_c of 106.29 K.

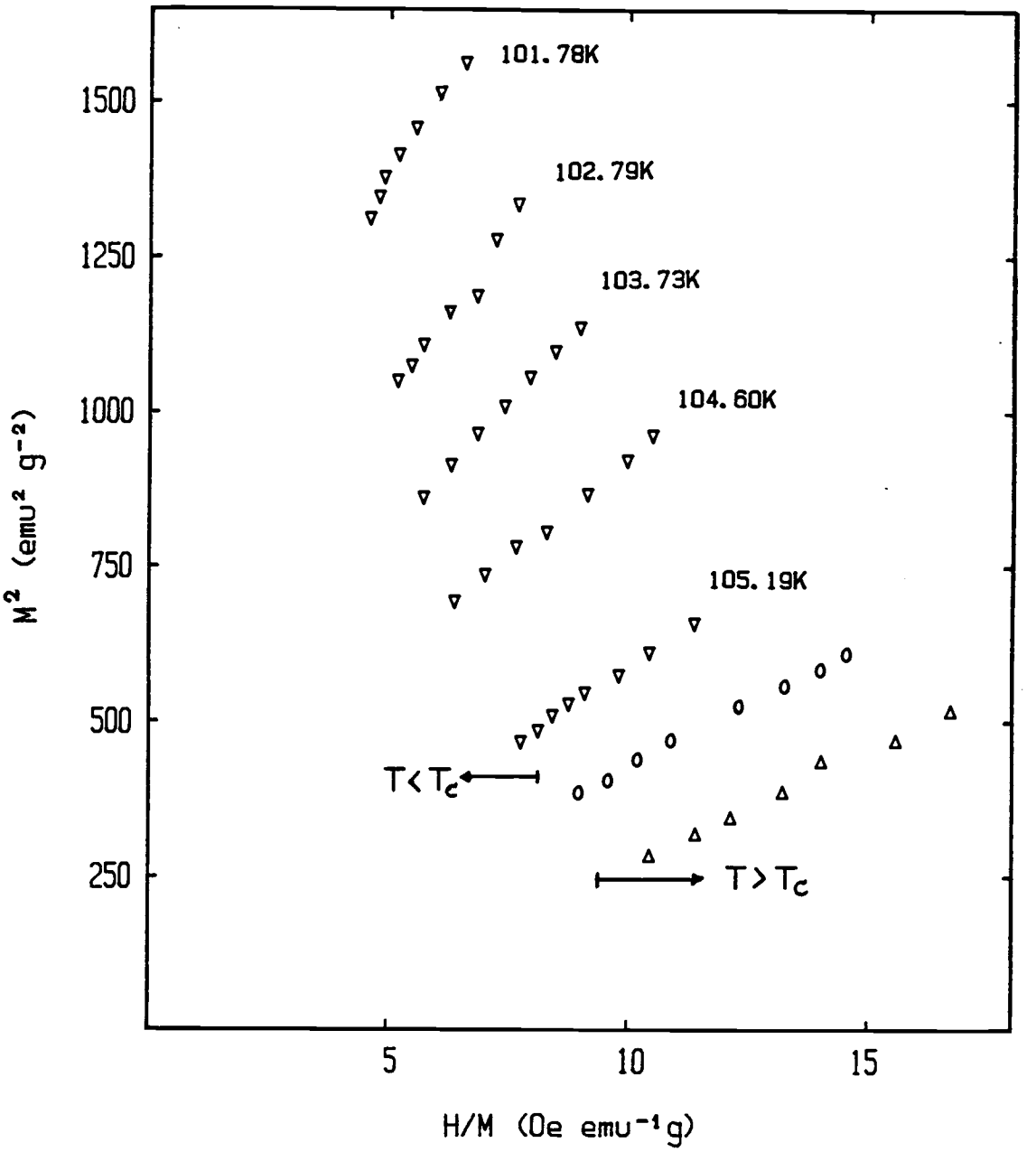

FIGURE 14: Arrott-Kouvel plots for temperatures $T \leq T_c$

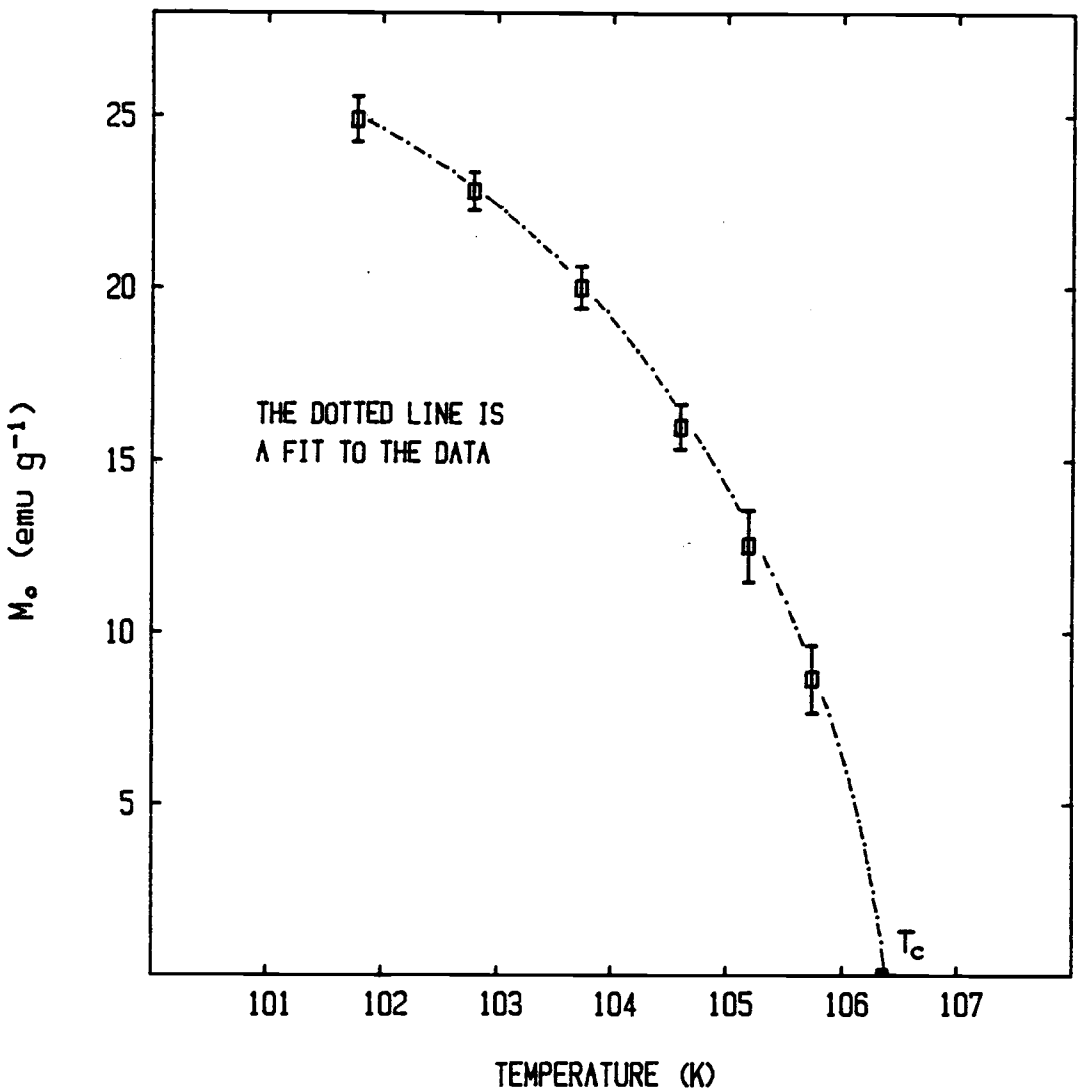

FIGURE 15: Spontaneous magnetization vs. temperature below the critical point

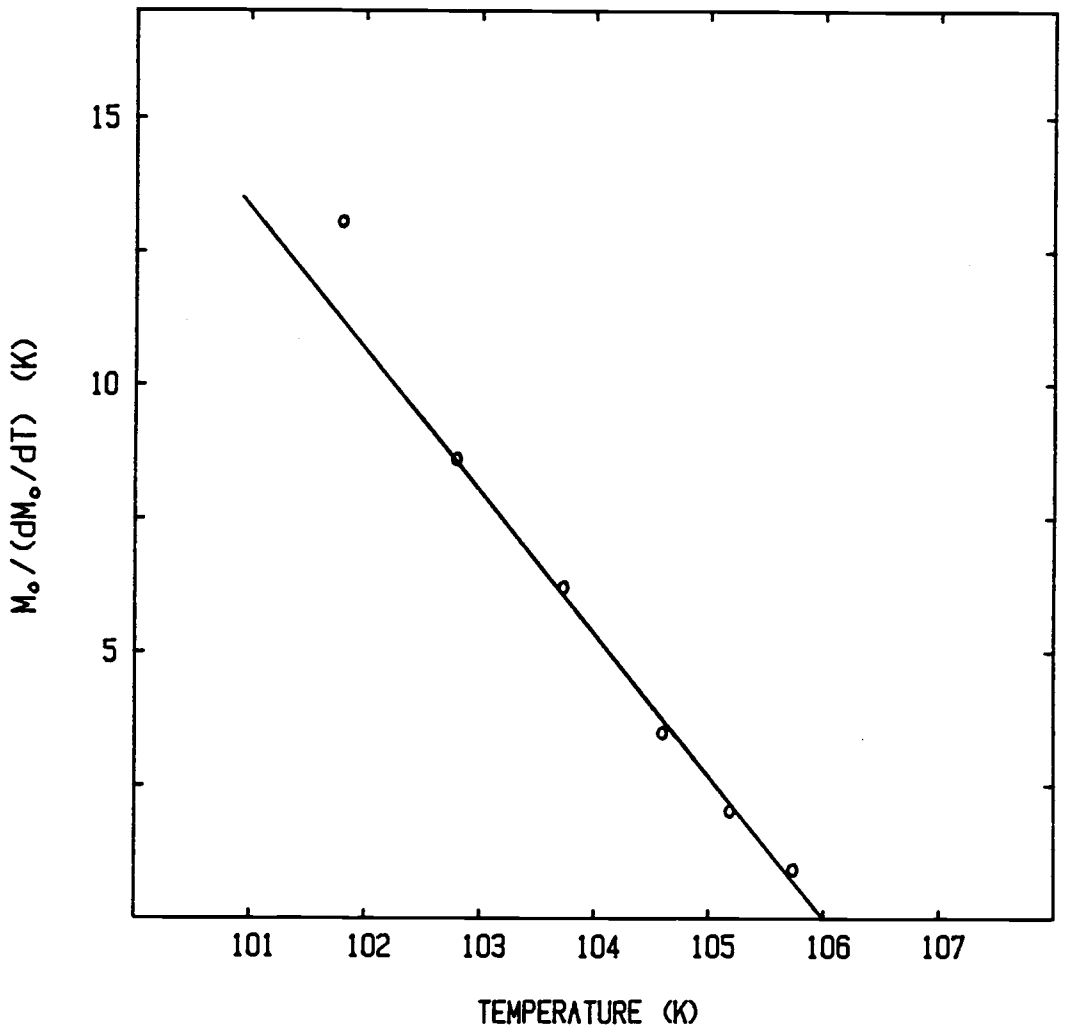

FIGURE 16: $M_0/\{dM_0/dT\}$ vs. T for the amorphous $Gd_{0.70}Pd_{0.30}$ sample. Least-mean-squares fit to the five uppermost data points is: $M_0/\{dM_0/dT\}=2.6694*T-282.9702$ with $r^2=0.9979$ yielding $\beta=0.374$ and $T_c=106.00$ K.

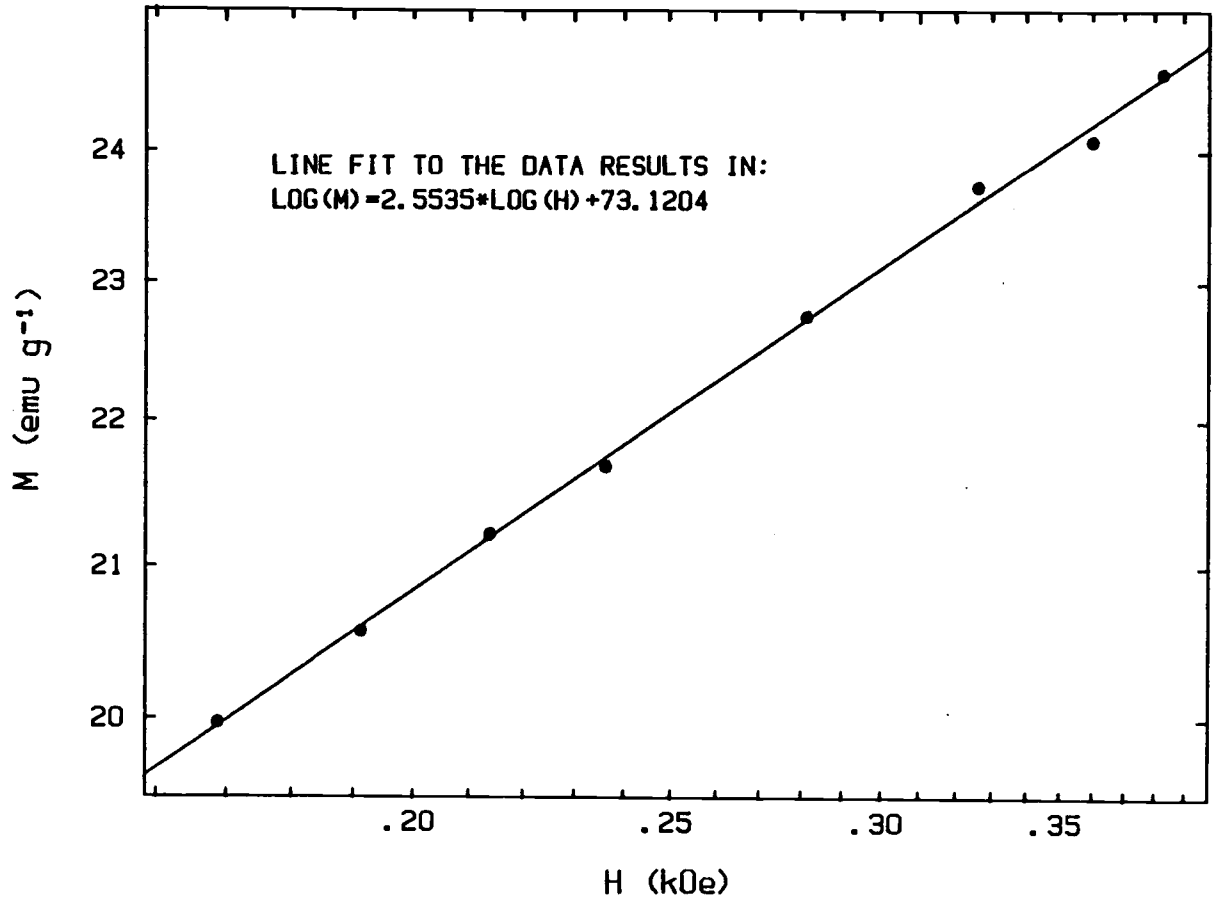

FIGURE 17: Specific magnetization M of sputtered amorphous $Gd_{0.70}Pd_{0.30}$ vs. applied magnetic field H at the critical isotherm (T = 106.34 K)

For temperatures 101 < T < 106 K, further Arrott plots were accomplished, this time in order to determine the specific magnetization. It was found here, as in previous work by others, that it is generally easier to determine χ_0^{-1} = H/M than the spontaneous magnetization; in one sense this is due to large gradients in $M^2(H/M)$ at small magnetic field values and in another part due to experimental difficulties stemming from the fact that the magnetic field could not be lowered much below 160 Oe, making accurate extrapolation to H/M = 0 extremely difficult. FIGURE 14 shows Arrott-Kouvel plots for the region $T \leq T_c$, and in FIGURE 15 the results of the extrapolation are graphed versus temperature. The magnetic exponent β is finally determined as the inverse of the slope in FIGURE 16. These data are not as good as those from which γ has been determined. From $M_0/\{dM_0/dT\}$ as a function of temperature near T_c, a value of β = 0.374 is determined, and in fact it can be seen that extrapolation yields a T_c value of 106.00 K. Considering the degree of difficulty with the extrapolation of $M^2(H/M)$ and the possibility for further inaccuracy when determining not only M_0^2 but also dM_0/dT directly from the data, this difference in T_c does not seem unacceptably large (i.e. ~ 0.3 K). Because of this reason, however, the ferromagnetic Curie temperature has been identified with the higher value from the γ-data.

M(H) was determined at T = 106.34 K (essentially the critical isotherm), and FIGURE 17 gives the data in double logarithmic form, which yields a value for δ of 3.916.

Finally, the errors associated with fitting the data by straight lines gives rise to the assignment of the following values: $\gamma = 1.010 \pm 0.05$, $\beta = 0.374 \pm 0.04$, and $\delta = 3.916 \pm 0.08$. This set of exponents clearly satisfies the Widom scaling law $\gamma = \beta(\delta - 1)$ within the range of experimental error.

DISCUSSION

The results obtained in the measurements on sputtered amorphous $Gd_{0.70}Pd_{0.30}$ (CENS sample) can now be compared with results of the amorphous sample (same constituents and same atomic proportions) produced by liquid quenching at the Oak Ridge National Laboratory (ORNL sample). The question that arises is that of how the different methods of production will influence the critical behavior of amorphous $Gd_{0.70}Pd_{0.30}$. The results of both investigations are listed in TABLE 1:

	sputtered $Gd_{0.70}Pd_{0.30}$	liquid quenched $Gd_{0.70}Pd_{0.30}$
γ	1.010 ± 0.05	1.010 ± 0.09
β	0.374 ± 0.04	0.341 ± 0.02
δ	3.915 ± 0.08	3.95 ± 0.1
θ_p	132.20 K	155.20 K
T_c	106.29 K	131.77 K
$\theta_p - T_c$	25.91 K	23.43 K
α	+ 0.24	+ 0.30

TABLE 1: Summary of the results of two independent investigations on amorphous $Gd_{0.70}Pd_{0.30}$

The critical exponents as listed show identical values within the estimated error limits. The deviation in β can be explained by

graphical difficulties in the determination of M_0^2. while δ would be in agreement, taking once again the error range of both liquid quenched and sputtered samples into account. For the first time, it has been directly demonstrated that the critical exponents DO NOT reflect the different methods of preparation of an amorphous material, a result which confirms the general thought that the critical behavior is independent of the details of the atomic structure and depends only on the dimensionality of the system and the degrees of freedom of the magnetic fluctuations. The critical exponents of the CENS as well as the ORNL sample are found to obey the Widom scaling law, although the values as a group are not characteristic of any single model. While γ = 1.010 could be associated with a mean field theory, the value of β = 0.374 cannot. It appears that the magnetic exponent could be rather well described with the Heisenberg model which predicts a value of 0.33.

The most striking difference, however, arises in the critical temperature which, for the sputtered material, is shifted by roughly 26 K towards a lower value. The explanation for a lowered critical point has to be sought in the different production process of the sample. It is possible to predict the paramagnetic Curie temperature, θ_p, of amorphous Gd_xM_{1-x} theoretically. Calculations on the basis of an exponentially damped RKKY (Rudermann-Kittel-Kasuya-Yosida) interaction (ref. 13), presume only the nearest neighbor interaction to be important. Differences in the "amor-

phousness" of the sample, as they might arise due to different methods of preparation, are also taken into account.

$$\theta_p = \frac{S(S+1)}{3k_B} \rho_0 \int J_{eff}(R) g(R) d^3R \tag{30}$$

where ρ_0 is the density of magnetic atoms, S the spin of the Gd-ion, and g(R) the pair distribution function. The effective exchange coupling $J_{eff}(R)$ was discussed by Kaneyoshi (ref. 14) approximately, especially for a system in which the electronic mean free path is about the average nearest-neighbor distance;

$$J_{eff}(R) = \frac{(J_{s-d})^2}{E_F} \frac{k_F^6}{8} \tag{31}$$

with

$$F(R) = \frac{1}{(2k_F R)^4} [(1 + \alpha R)\sin\beta R - \beta R \cos \beta R] e^{-\alpha R} \tag{32}$$

and are parameters defined by:

$$= 2k_F (1 + y^2)^{1/4} \cos (\phi/2 + \pi/4) \tag{33}$$

$$= 2k_F (1 + y^2)^{1/4} \cos (\phi/2 - \pi/4) \tag{34}$$

$$= \arctan (E_F/\Gamma) = \arctan (y^{-1}), \text{ where}$$

k_F is the Fermi wave vector of the conduction electrons; E_F the Fermi energy; Γ, a parameter characterizing the disorder of a system; and J_{s-d}, a coupling constant between s- and d-electrons. In the case of $y = 0$ the interaction reduces to the usual RKKY result. Substituting equation (31) into equation (30), the paramagnetic Curie temperature becomes, after partial integration,

$$\theta_p = \frac{S(S+1)\ (J_{s-d})^2}{4k_B} \cdot \rho_0 \int_0^\infty \frac{d}{dR} g(R)\ \frac{\sin\beta R}{R} e^{-\alpha R}\, dR \qquad (35)$$

The form of the pair distribution function, g(R), (probability of finding a second particle at a position R with respect to an arbitrary first particle) contains the information about the structure of the amorphous sample and can be modeled or determined by wide angle X-ray scattering. θ_p can then be evaluated numerically. However, it is not known yet how this might produce a shift of the paramagnetic Curie point.

Long-range order as the ferromagnetic Curie point is approached, may be dominated by the RKKY interaction. That is, the spins of the 4f-Gd cores are coupled together by the magnetization induced in the conduction electron gas of both ions and Pd. The indirect exchange interaction between highly localized 4f electrons via the conduction electrons has an essential consequence: The spin on an atom may be regarded as setting up a spin polarization in the conduction electrons. This polarization couples to the spins of

other atoms to produce an effective exchange with long range order. On the other hand, so great an extension of the long range order over approximately 8 K in the vicinity of the critical point in the presence of an electronic mean free path of order of the interatomic spacing cannot be explained. Although this effect has been seen in a number of works on the critical exponents of amorphous systems, so far no satisfactory theoretical treatment of the phenomenon exists.

For amorphous Gd-containing systems γ values are among the smallest observed. The γ value of 1.010 is compatible with a recent theoretical model calculation by Fahnle et al. (ref. 15). The basis of this model is an enhanced molecular field theory where the interaction energy of a spin at site i with all the spins at sites j is approximated by the interaction of the spin with the thermal averages, $\langle S_j \rangle$. The molecular field Hamiltonian

$$H_{mf} = \sum_i \sum_j J_{ij} \langle S_j \rangle \langle S_i(t) \rangle \tag{36}$$

thus, contains only the fluctuations of the spins at site i, whereas the time-fluctuations of spins at site j are averaged out. The enhancement of this theory is approached via a spatially correlated magnetization which in the continuum limit ($\langle S_j \rangle \rightarrow S(r')$; $M(r') = g\mu_B S(r')$ with g = Landé factor and μ_B = Bohr's magneton; $J_{ij} \rightarrow J(r,r')$ exchange interaction constant) is given by

$$M(r')_{corr} = \int f(r'-r'', \zeta(T)) M(r'') d^3r'' \tag{37}$$

where $\zeta(T)$ is the thermal correlation length. The integral kernel f(....) is to average out irrelevant fluctuations of the magnetization M(r"), and for $T \to T_c$ it is a slowly-varying function in space. Therefore, the correlations should be about constant in the whole sample as in the homogeneous molecular field theory. However, for very high temperatures the kernel describes the spatial fluctuations as in the inhomogeneous field theory. The calculations finally predict a temperature dependent exponent $\gamma(T)$ which starts at a mean field value of unity at $T = T_c$ and runs through a maximum as the temperature is increased. In the high temperature limit the model once again gives an asymptotic value of 1. In this work, however, $\gamma(T)$ is constant over a range of $T - T_c \sim 8$ K and then starts to increase to higher values than predicted by theory. This behavior is shown in FIGURE 18 where $\gamma(T)$ is plotted against the reduced temperature, T/T_c-1. It should be noted that for amorphous materials one expects an increase in γ with temperature, while in the case of crystalline materials γ has been found to decrease (ref. 16).

The unusually wide temperature range of approximately 25 K between paramagnetic and ferromagnetic Curie point was observed in both CENS and ORNL samples, and values for the inverse mass specific susceptibility are much the same in either case, increasing by a factor of 100 compared with values in the paramagnetic regime. In turn the local moment just around T_c is enhanced above μ_{Gd}.

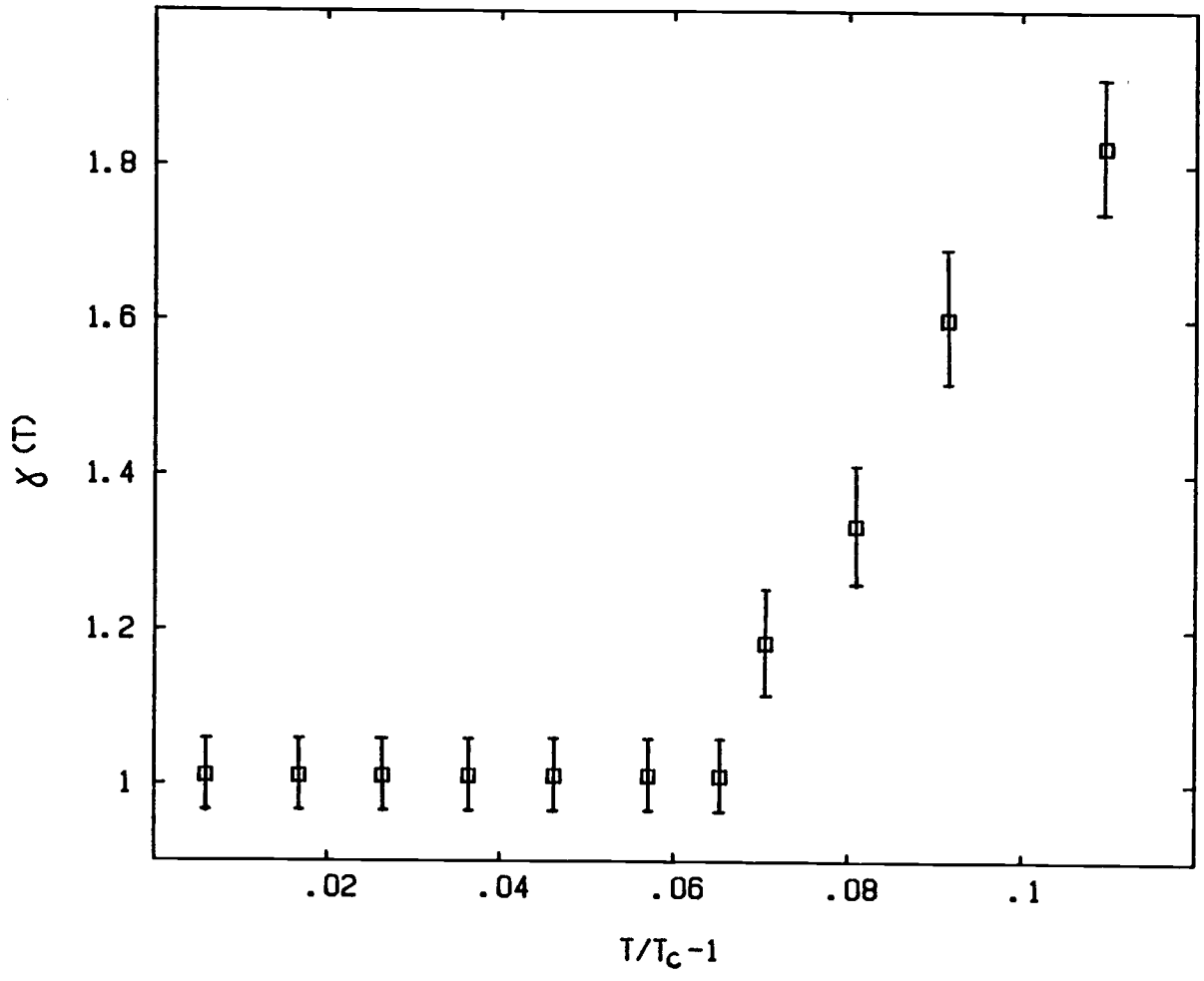

FIGURE 18: $\gamma(T)$ as a function of reduced temperature

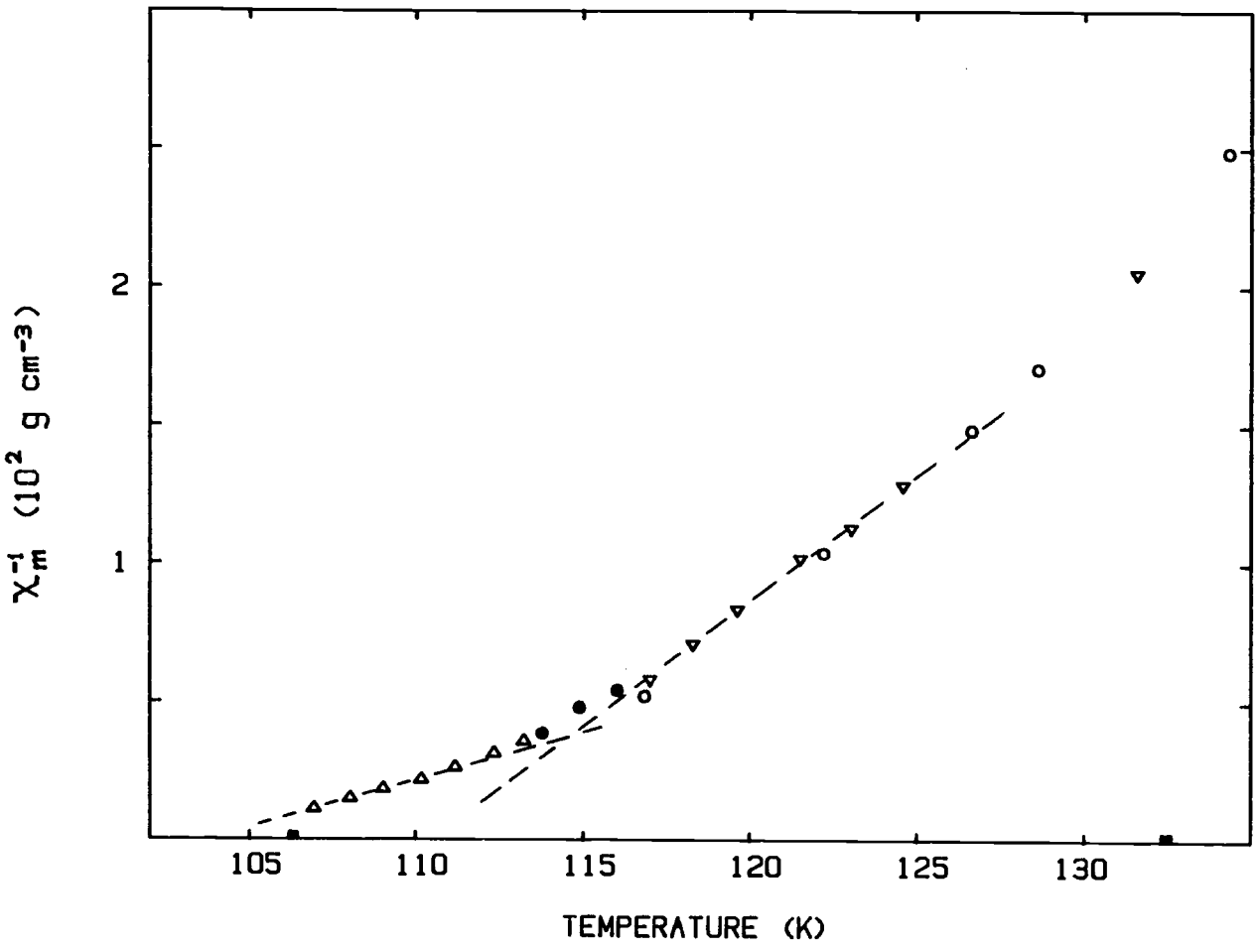

FIGURE 19: Curie Weiss plot enlarged for temperatures $T \leq 135$ K.

This might be indicative of superparamagnetic behavior above T_c. That is, as the critical temperature is approached, ferromagnetic clusters with enhanced local magnetic moments and possible correlations among such clusters are built up, (ref. 17) and (ref. 18). Close examination of magnetic susceptibility data in the region below 135 K, shown in FIGURE 19, seems to reveal quasi-Curie Weiss behavior as evidenced by linear regions in χ_m^{-1}.

So far, only the directly measured results have been discussed. However, on the basis of the scaling law hypothesis (discussed earlier in the theory section) one can predict other critical exponents. One such exponent is α, which has been associated with the critical behavior of the zero field specific heat $C_{H=0}$. α was found, using the Rushbrooke equality ($2 = \alpha + 2\beta + \gamma$) to be positive in both, the ORNL and CENS sample. This result is unusual in so far as most work on amorphous rare-earth and transition metal alloys reveals a negative specific heat exponent. In a review article on magnetic amorphous alloys by Egami (ref. 16) the meaning of $\alpha > 0$ ("type I" or "inhomogeneous case"), and $\alpha < 0$ ("type II" or "homogeneous case") is discussed. For a well defined transition in a random, but macroscopically homogeneous system the critical index is negative. Harris (ref. 19) and Lubensky (ref. 20) report: $\alpha < 0$ is a necessary condition for a homogeneous phase transition to occur in a disordered material; on the other hand $\alpha > 0$ guarantees that the system is not homogeneous.

Kadanoff et al. (ref. 2) discuss various instances in which $\alpha > 0$. However, it is not possible to compare experimental results cited there with those presented in this work. Firstly, because the systems are quite different, including ferro-electrics, and secondly, because the samples were crystalline. Furthermore, it is to some extent ambiguous to discuss the meaning of a sharp or smeared phase transition on the basis of a critical index derived by the scaling law hypothesis, without having first-hand specific-heat data.

X-ray scattering from the CENS $Gd_{0.70}Pd_{0.30}$ specimen was conducted in both small and wide angle regimes. The wide angle results, shown in FIGURE 6, confirm the absence of microcrystallites - a result in agreement with that of the edge portions of the fastest ORNL liquid-quenched sample. The data yield a mean separation for Gd-Gd (Gd-Pd) of 4.47 Å. This value is significantly greater than that associated with the ORNL sample, may be due to hydrogen content in the sample and is compatible with a reduction in the overall coupling strength between Gd atoms, assuming that it proceeds via the indirect RKKY interaction.

On the other hand, the small-angle X-ray scattering (SAXS), shown in FIGURE 7, results from inhomogeneities within the $Gd_{0.70}Pd_{0.30}$ alloy at which the local electronic density is sufficiently different from that associated with the global $Gd_{0.70}Pd_{0.30}$ background matrix.

The overall "structure" of the distribution of inhomogeneities in real space is the convolution of a function describing the electronic distribution of the basic scattering entity and a function describing its repetition (in this case one can characterize the mean separation between inhomogeneities). As a result, the required Fourier transform is simply the product of the individual transforms of the two functions.

$$I(k) = A \left[\frac{\sin kr_s - kr_s \cos kr_s}{(kr_s)^3} \right]^2 * \left[1 + \int_0^\infty 4\pi r^2 [P(r) - 1] \frac{\sin kr}{kr} \, dr \right] \qquad (38)$$

Here the Rayleigh formula (ref. 21) for scattering from a sphere of radius r_s has been chosen as the structure factor and the Debye approximation (ref. 22) will be assumed in the radial pair disribution function P(r), resulting in a finite value of r_0, equal to the mean interparticle separation distance, being assigned to the upper limit of integration.

$$I(k) = A \left[\frac{\sin kr_s - kr_s \cos kr_s}{(kr_s)^3} \right]^2 * \left[1 - \frac{3 [\sin kr_0 - kr_0 \cos kr_0]}{(kr_0)^3} \right] \qquad (39)$$

The dashed curve (FIGURE 8) results from a choice of "spherical" inhomogeneity having a radius of 6.5 Å and being separated from its neighbors by a mean distance of 50 Å.

The agreement is rough but sufficient to provide a good indication of the value of these two parameters. The predicted curve is most free of scatterer shape considerations at smallest k values and it is here that the agreement between measurements and model is best. The $Gd_{0.70}Pd_{0.30}$ undergoes resonance fluorescence when bombarded by Ni filtered Cu Kα X-rays and so there is a constant background level at all angles (s-values measured) which had to be subtracted from the measured values. Any error in the assessment of this constant value has an enormous relative effect on the corrected curve (FIGURE 8) at larger s-values where the experimental count levels are low. For this reason as well, it is best to go with the fit at lowest s-values ($0 \leq s \leq 0.06$ Å^{-1}).

While no unique specifications of the chemical nature of these inhomogeneities can be made on the basis of these X-ray measurements alone, these results do provide additional evidence for the existence of possible paramagnetic clusters in sputtered $Gd_{0.70}Pd_{0.30}$.

SUMMARY

The critical behavior of sputtered amorphous $Gd_{0.70}Pd_{0.30}$ was studied and three critical exponents were independently determined. The results were compared with previous work on the same alloy produced by liquid quenching. The findings are:

(1) Both, sputtered and liquid quenched samples possess much the same critical exponents (β, γ, δ), independent of the method of preparation. The results are summarized in TABLE 1. As in the liquid-quenched case, the set of critical exponents for the sputtered specimen was seen to obey Widom's scaling law $\gamma = \beta (\delta - 1)$.

(2) The ferromagnetic Curie point T_c, associated with the phase transition, is shifted towards lower temperatures in the case of the sputtered sample. This is compatible with wide angle X-ray scattering data which indicate that the mean Gd-Gd (Gd-Pd) separation is greater in the sputtered material than in the liquid-quenched specimen.

(3) The spread between paramagnetic (θ_p) and ferromagnetic Curie point (T_c) is large in both samples. One may argue that this large range of temperature arises from the occurrence of superparamagnetism in $Gd_{0.70}Pd_{0.30}$ for $T > T_c$.

(4) Application of the scaling law ($2 = \alpha + 2\beta + \gamma$) was made, in order to determine the critical exponent associated with the zero field specific heat, $C_{H=0}$. α was found to be positive which is compatible with the presence of small scale inhomogeneities.

(5) Confirmation of the existence of superparamagnetic clusters in $Gd_{0.70}Pd_{0.30}$ should be provided by two types of additional experiments: (i) susceptibility behavior of sputtered Gd-Pd over a wide range of relative Gd/Pd concentrations and (ii) angular and energy dependence of magnetic neutron scattering. The first-mentioned experiments are ones that could be conducted at Oregon State University and would require only small amounts of sputtered Gd-Pd having various Gd and Pd concentrations. The second set of experiments requires large amounts of sputtered Gd-Pd material and would have to be carried out at a national low-angle neutron scattering facility such as the Oak Ridge National Laboratory in this country or the Institute Laue-Langevin in Grenoble, France.

BIBLIOGRAPHY

1. Griffiths, D. J., D. S. Easton, D. M. Kroeger, "Critical Exponents of Amorphous $Gd_{0.70}Pd_{0.30}$," Physical Review B, Vol. 31, Number 1, p. 287, 1985.

2. Kadanoff, L., W. Gotze, D. Hamblen, R. Hecht, E. Lewis, V. Palciauscas, M. Rayl, J. Swift, D. Aspens, J. Kane, "Static phenomena near critical points: Theory and experiment," Review of Modern Physics, Vol. 39, Number 2, p. 395, 1967.

3. Fisher, M. E., "The Theory of Equilibrium Critical Phenomena," Reports on Progress in Physics, Vol. 30 (pt. 2), p. 615, 1967.

4. Ashcroft, N. W. and D. N. Mermin, Solid State Physics, Holt, Rinehart and Winston, 1976.

5. Kittel, C., Introduction to Solid State Physics. John Wiley & Sons, 1976.

6. Stanley, E. H., Introduction to Phase Transitions and Critical Phenomena, Oxford University Press, 1971.

7. Arrott, A., "Criterion for Ferromagnetism from Observation of Magnetic Isotherms," Physical Review, Vol. 108, Number 6, p. 1394, 1957.

8. Kouvel, J. S., General Electric Research Laboratory, Rep. Number 57-RL-1799, 1957 (unpublished).

9. Lindoy, L. F. and V. Katovic, "A Variable Temperature Faraday Magnetic Balance," Journal of Chemical Education, Vol. 49, Number 2, p. 117, 1972.

10. Lewis, J., and R. G. Wilkins, Modern Coordination Chemistry, Interscience Publishers, Inc., 1960 (Chapter 6).

11. Poon, S., and J. Durand, "Critical Phenomena and Magnetic Properties of an Amorphous Ferromagnet: Gadolinium-gold," Physical Review B, Vol. 16, Number 1, p. 316, 1977.

12. Gardner, W., J. Penfold, and T. F. Smith, "The Magnetic Properties of Rare-earth Pd-phase," Journal of Physics F, Vol. 2, p. 133, 1972.

13. Kaneyoshi, T., Amorphous Magnetism, CRC Press, Inc., 1984.

14. Kaneyoshi, T., "Indirect Exchange in a Disordered Magnet," Journal of Physics F, Vol. 5, p. 1014, 1975.

15. Fahnle, G., G. Herzer, R. Kronmuller, R. Meyer, M. Saile, and T. Egami, "The Magnetic Phase Transition in Amorphous Ferromagnets and in Spin Glasses," Journal of Magnetism and Magnetic Materials, Vol. 38, p. 240, 1983.

16. Egami, T., "Magnetic Amorphous Alloys: Physics and Technological Applications," Reports on Progress in Physics, Vol. 47, Number 12, p. 1601, 1984.

17. Yamamoto, H., H. Onodera, T. Hosoyama, T. Masumoto, H. Yamauchi, "Magnetic Inhomogenuity in Amorphous Fe-Zr Alloys," Journal of Magnetism and Magnetic Materials 31-34, p. 1579, 1983.

18. Acker, F., and R. Huguenin, "Ferromagnetism in V-Ni, Pt-Ni and Pd-Ni Alloys," Journal of Magnetism and Magnetic Materials, Vol. 12, p. 58, 1979.

19. Harris, A. B., "Effects of Random Defects on the Critical Behavior of Ising Models," Journal of Physics C, Vol. 7 (pt. 2), p. 1671, 1974.

20. Lubensky, T.C., "Critical Properties of Random-spin Models from the ε-Expansion," Physical Review B, Vol. 11 (pt. 3), p. 3573, 1975.

21. Rayleigh, Lord: "The Incidence of Light upon a Transparent Sphere of Dimensions Comparable with the Wave-length," Proceedings of the Royal Society (London), Vol. A 84, p. 25, 1911.

22. Debye, P., "Zerstreung von Rontgenstrahlen," Annalen der Physik, Vol. 46, p. 809, 1915.

23. Arrott, A., and J. E. Noakes, "Approximate Equation of State for Nickel Near its Critical Temperature," Physical Review Letters, Vol. 19, Number 14, p. 786, 1967.

24. Ma, S. K., "Introduction to Renormalization Group," Review of Modern Physics, Vol. 45, Number 4, p. 589, 1973.

25. Yamada, K., Y. Ishikawa, Y. Endoh, and T. Masumoto, "The Magnetic Phase Transition of an Amorphous Fe-P-C and its Alloys Containing Ni and Cr," Solid State Communications, Vol. 16, p. 1335, 1975.

26. Wagner, D., and E. P. Wohlfarth, "Magnetic Isotherms of Heterogeneous Ferromagnets," Physica 112 B, p. 1, 1982.

27. Rado, G. T., and H. Suhl, Magnetism (Vol. 2II), Academic Press, 1965.

28. Goldfarb, R. B., and C. E. Patton, "Superparamagnetism and Spin-glass Freezing in Ni-Mn Alloys," Physical Review B, Vol. 24, Number 3, p. 1360, 1981.

APPENDICES

Appendix I: Relationships for Raw Data Processing

The coordinate system (Figure A1) shows the relative orientations of the applied d.c. magnetic field and the respective gradient field.

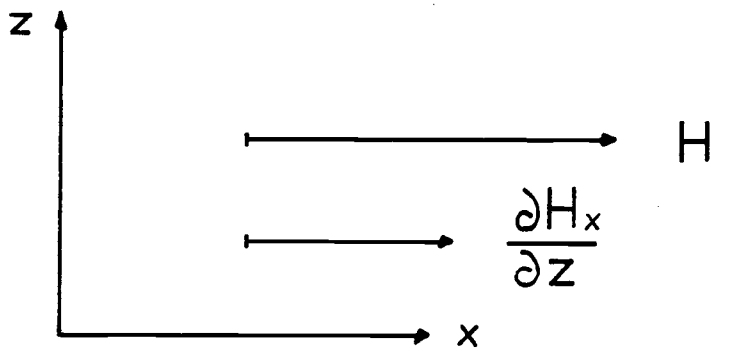

FIGURE A1: Relative coordinates of magnetic field and respective gradient field

The magnetic moment in x - direction is given by

$$\mu_x = \chi_m Hm_s \qquad \text{(A 1.1)}$$

while

$$\mu_y = \mu_z = 0 \qquad \text{(A 1.2)}$$

due to the homogeneity of the d.c. magnetic field. Furthermore, the force experienced by the sample in an inhomogeneous magnetic field in respect to the cartesian coordinates is:

$$F_\beta = \mu_\alpha \frac{\partial H_\beta}{\partial x_\alpha} \qquad \text{(A 1.3)}$$

where α and β denote x, y, and z direction respectively. As a consequence of (A 1.1) and (A 1.2) only the components

$$F_x = \mu_x \frac{\partial H_x}{\partial x} \qquad \text{(A 1.4a)}$$

$$F_y = \mu_x \frac{\partial H_y}{\partial x} \qquad \text{(A 1.4b)}$$

$$F_z = \mu_x \frac{\partial H_z}{\partial x} \qquad \text{(A 1.4c)}$$

survive. Those can be further reduced, since according to Ampere's Law $j_y = 0$.

$$\frac{\partial H_x}{\partial z} = \frac{\partial H_z}{\partial x} \qquad \text{(A 1.5)}$$

And also the geometry of the gradient field guarantees that

$$\frac{\partial H_x}{\partial x} = \frac{\partial H_y}{\partial x} = 0 = \frac{\partial H_x}{\partial y} \qquad \text{(A 1.6)}$$

This leaves only one force component:

$$F_z = \mu_x \frac{\partial H_x}{\partial z} = \chi_m H m_s \frac{\partial H_x}{\partial z} \qquad \text{(A 1.7)}$$

where χ_m is the mass specific susceptibility and m_s denotes the mass of the sample. In static equilibrium, however, this force is just equal to force exerted due to gravity, and one may write:

$$F_z = g \Delta m \qquad \text{(A 1.8)}$$

or solving for χ_m gives:

$$\chi_m = \frac{g\ \Delta m}{2m_s H\ \{\partial H_x/\partial z\}} \qquad \text{(A 1.9)}$$

The factor 2 arises from the fact, that Δm is strictly speaking the sum of change in weight in positive and negative z-direction as the gradient field is reversed. In addition, a correction term, accounting for the diamagnetic contribution of the quartz sample holder must be added so that

$$\Delta m \rightarrow \Delta m - \Delta m_{QB} \qquad \text{(A 1.10)}$$

The sign convention for Δm will be used in the usual sense so that diamagnetic contributions to the magnetic susceptibility are taken into account by a negative sign in Δm, and paramagnetic, ferromagnetic, etc. with a positive sign. Δm is measured directly in the experiment, while Δm_{QB} has to be determined separately at various magnetic field strengths.

For magnetization measurements (A 1.1) in connection with (A 1.10), or the mass specific magnetization

$$M = \chi_m H \qquad \text{(A 1.11)}$$

can be utilized. It is important to note that throughout this work the mass specific magnetization (denoted by a capital M) has been used.

Appendix II: Choice of Unit System

The quantities used in the above analysis as well as for previous calculations and graphs are based on the cgs - emu unit system; i.e. the permeability of a vacuum μ_0 is omitted from magnetophysical formulas because in this system it is equal to one and has no dimensions. The units for respective quantities are as follows:

$$H\ [\text{Oersted} = g^{1/2}\ s\ cm^{1/2}] \qquad (A\ 2.1)$$

which gives for

$$\chi_m\ [cm^3\ g^{-1} = \text{emu}\ g^{-1}\ Oe^{-1}] \qquad (A\ 2.2)$$

with 1 electromagnetic unit: $\text{emu} = g^{1/2}\ cm^{5/2}\ s^{-1}$ (A 2.3)

In this fashion the appropriate units for the mass specific magnetization are readily established.

$$M\ [\text{emu}\ g^{-1}] \qquad (A\ 2.4)$$

Appendix III: Temperature and Gradient Field Calibration

The temperature sensing Si diode (Lakeshore Cryotronics, Model DT-500 KL) was calibrated prior to its use, and compared to a factory calibrated diode with the same specifications. Three characteristic temperatures - liquid Nitrogen, freezing point of water, and room temperature - seemed to be sufficient to establish the relationship between diode voltage and temperature. The temperature readings were done by means of a calibrated thermocouple. FIGURE A2 shows this voltage - temperature characteristic.

The magnetic field and gradient field were calibrated earlier by G. L. Robbins (Chemistry Department) using an EPR and NMR gaussmeter. In this way a complete field mapping was obtained, and the maximum of the product of d.c. magnetic field and gradient field was set. Nevertheless, the gradient field was checked for a current setting of 30 Amp using a NBS Aluminum standard with known susceptibility. The weight change for normal and reversed gradient field was determined as a function of applied field. The slope found in a plot Δ m vs. H is directly proportional to the gradient field. Agreement with previous calibrations by D. Griffiths and G. L. Robbins in the order of 3% have been verified. The discrepancy stems from the fact that too much background noise caused by a recently installed air circulating system made a more accurate determination impossible.

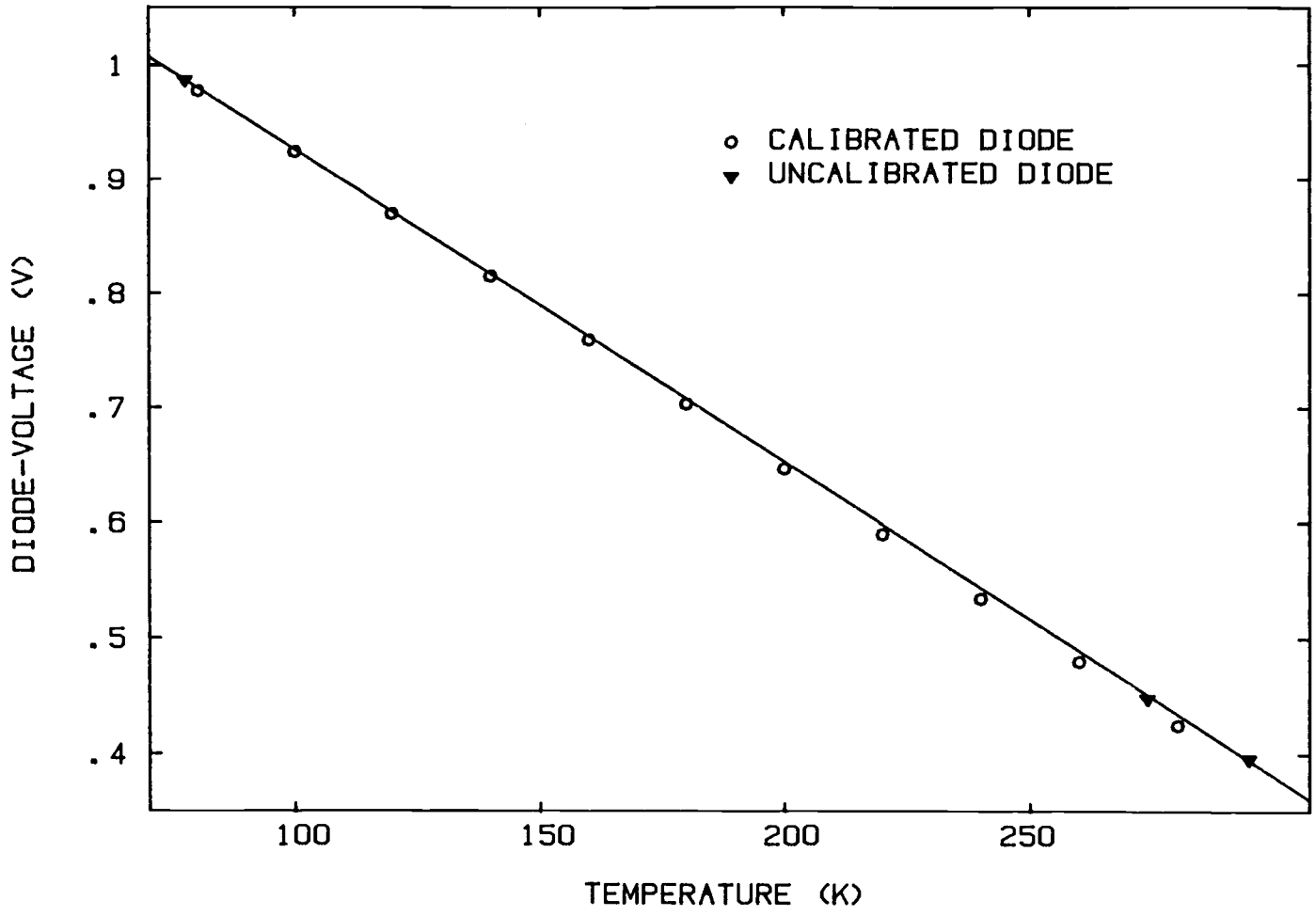

FIGURE A2: Calibration curve for the temperature sensing Si-diode